Analysis of Generator Fault Ride Through Capability

Master Thesis

submitted to

Institute of Electrical Power Systems
Graz University of Technology

by

Lejla Halilbasic

Supervisor
Dipl.-Ing. Johann Hell
Ao.Univ.-Prof. Dipl.-Ing. Dr.techn Herwig Renner

Institutsleiter: Univ.-Prof. DI Dr.techn. Lothar Fickert

A - 8010 Graz, Inffeldgasse 18-I
Telefon: (+43 316) 873 – 7551
Telefax: (+43 316) 873 – 7553
http://www.ifea.tugraz.at
http://www.tugraz.at

Graz / June – 2015

In cooperation with:

EIDESSTATTLICHE ERKLÄRUNG

Ich erkläre an Eides statt, dass ich die vorliegende Arbeit selbstständig verfasst, andere als die angegebenen Quellen/Hilfsmittel nicht benutzt, und die den benutzten Quellen wörtlich und inhaltlich entnommene Stellen als solche kenntlich gemacht habe.

Graz, am 30.05.15

……..
Unterschrift

STATUTORY DECLARATION

I declare that I have authored this thesis independently, that I have not used other than the declared sources / resources, and that I have explicitly marked all material which has been quoted either literally or by content from the used sources.

Graz, 30 May 2015

……..
signature

Kurzfassung

Für die Simulation von Störfällen in elektrischen Netzen stehen eine Vielzahl an Werkzeugen mit unterschiedlichen Simulationsmethoden zur Verfügung. Diese können entsprechend ihres Detaillierungsgrades eingeteilt werden. Für ausgedehnte Netze kommen hauptsächlich vereinfachte Modelle zum Einsatz, welche die Ordnung des Gesamtsystems reduzieren und somit die Rechenzeit erheblich vermindern. Ein- und Mehrmaschinenprobleme werden mithilfe von komplexeren und detaillierten Modellen nachgebildet und untersucht.

Die zwei genannten Modellierungsansätze werden anhand eines konkreten Beispiels verglichen. Das Verhalten von Rohrgeneratoren bei Spannungseinbrüchen im Netz wird mit Hinsicht auf die Netzanschlussregeln des nordischen und deutschen Grid Codes untersucht. Solche Maschinen zeichnen sich durch eine sehr geringe Schwungmasse aus, die sich negativ auf die Stabilität auswirkt. Allerdings dürfen am Netz angeschlossene Erzeugungseinheiten bei definierten Spannungseinbrüchen weder instabil noch vom Netz getrennt werden.

Um diese Forderungen zu erfüllen, wird beim betrachteten Maschinensatz die Lösung mit einem Widerstand, der im Störfall zwischen Generator und Netz geschaltet wird, untersucht. Dieser wirkt während eines Spannungseinbruches der Beschleunigung des Rotors, hervorgerufen durch eine verminderte Leistungsabgabe, entgegen und verhindert somit ein Außertrittfallen des Generators.

Für die vereinfachte Simulation kommt dabei *DIgSILENT PowerFactory* zum Einsatz, wohingegen der detailliertere Ansatz mithilfe von *OpenModelica* verfolgt wird.

Schlüsselwörter: OpenModelica, DIgSILENT PowerFactory, RMS-Simulation, Grid Codes, Low-Voltage-Ride-Through, Rohrgenerator, Widerstandsbremse

Abstract

There are numerous tools for simulations of fault events in electrical grids based on various modelling approaches which can be grouped according to their level of detail. Simplified methods are usually applied to large and wide-stretching grids in order to reduce the order of the system and hence, the computing time. Single machine systems, on the contrary, are examined using more detailed and complex models.

The two modelling approaches are applied to a specific example and compared within the scope of the work. The dynamic response of bulb generators to voltage depressions in the grid is examined with regard to grid connection requirements from the Nordic as well as German grid codes. Bulb generators are characterized by very low inertia, thereby exhibiting a negative impact on system stability. According to low voltage ride through specifications, however, all grid connected generating units have to remain in synchronism and connected during pre-defined voltage sags.

This thesis examines a possible solution to enhance LVRT capabilities where a resistor is inserted between generator and grid in the event of a fault. The ohmic component acts as a brake reducing the acceleration of the rotor which is induced by an imbalance between dissipated and generated power during voltage sags, and thereby, avoiding the machine to loose synchronism with the power system.

DIgSILENT PowerFactory is used for demonstrations of simplified modelling approaches whereas *OpenModelica* serves as an example for detailed simulations.

Keywords: OpenModelica, DIgSILENT PowerFactory, RMS-simulation, Grid Codes, Low-Voltage-Ride-Through, Bulb generator, Series Braking Resistor

Abbreviations

Abbreviation	Description
AVR	Automatic Voltage Regulator
BPA	Bonneville Power Administration
BR	Braking resistor
CB	Circuit breaker
CP	Connection point
d-axis	Direct axis
EMT	Electromagnetic Transients
ENTSO-E	European Network of Transmission System Operators for Electricity
FRT	Fault Ride Through
GC	Grid Code
HV	High voltage
LV	Low Voltage
LVRT	Low Voltage Ride Through
NW	Northwest
oe	Over-excited
pf	Power factor
p.u.	per unit
PCC	Point of common coupling
PI	Proportional-Integral
PSS	Power System Stabilizer
q-axis	Quadrature axis
RMS	Root mean square
ROR	Run-Of-The-River hydroelectricity
SBR	Series braking resistor
TSO	Transmission System Operator
ue	Under-excited

Notations

Symbol	Unit	Description
$\gamma_{x,HV}$	p.u.	Share of transformer short circuit resistance on HV side
$\gamma_{R,HV}$	p.u.	Share of transformer short circuit reactance on HV side
$\Delta\omega$	rad/s or p.u.	Deviation of actual angular velocity from nominal value
η_h	%	Hydraulic efficiency
ϑ_{el}	deg or rad	Electrical rotol angle
ϑ_m	deg or rad	Mechanical rotol angle
Θ	deg or rad	Polar angle
λ	-	Local loss coefficient
ψ_d	p.u.	Synchronous stator flux component in d-axis
ψ_d'	p.u.	Transient stator flux component in d-axis
ψ_d''	p.u.	Subtransient stator flux component in d-axis
ψ_D	p.u.	Damper winding flux component in d-axis
ψ_{fd}	p.u.	Field flux
ψ_q	p.u.	Synchronous stator flux component in q-axis
ψ_q'	p.u.	Transient stator flux component in q-axis
ψ_q''	p.u.	Subtransient stator flux component in q-axis
ψ_Q	p.u.	Damper winding flux in q-axis
ω	rad/s or p.u.	Electric angular velocity
ω_0	rad/s or p.u.	Nominal value of electric angular velocity
ω_{Gen}	rad/s or p.u.	Generator mechanical angular velocity
ω_{Tur}	rad/s or p.u.	Turbine mechanical angular velocity
a	m/s	Wave speed
A	m^2	Pipe cross-section
c	-	Voltage factor
c	rad^{-1}	Spring constant
cos(φ)	-	Power factor
$\cos(\varphi_{Gen})$	-	Power factor at “Gen” bus bar
$\cos(\varphi_{PCC})$	-	Power factor at “PCC” bus bar
C	F	Capacitance
C’	F/m	Distributed capacitance
d	-	Damping constant
D	m	Pipe diameter
g	9,81 m/s^2	Gravitational acceleration
h	p.u.	Water head
H	s	Inertia time constant

H_0	m	Nominal water head
i_d	p.u.	Stator current in d-axis
i_D	p.u.	Current in damper winding (d-axis)
i_{fd}	p.u.	Field current
i_q	p.u.	Stator current in q-axis
i_Q	p.u.	Current in damper winding (q-axis)
J	kgm^2	Inertia
J_{Gen}	kgm^2	Generator inertia
J_{Tur}	kgm^2	Turbine inertia
J_{Total}	kgm^2	Total inertia
k_{sat}	-	Saturation factor of stator leakage reactance
i_0	%	No-load current
l	m	Length of pipe
L	H	Inductance
L’	H/m	Distributed inductance
n	-	Number of segments
N	rev/min	Rotational turbine speed
N_0	rev/min	Nominal speed
p	-	Number of poles
P_{Cu}	W	Copper losses
P_{Gen}	W	Generated active power
P_h	W	Hydraulic power
P_m	W	Mechanical power
P_{max}	W	Maximum active power
P_{P1}	W	Active power at bus bar P1
P_{PCC}	W	Active power at PCC
q	p.u.	Discharge
Q	m^3/s	Discharge
Q_0	m^3/s	Nominal discharge
Q_{Gen}	var	Generated reactive power
r_T	p.u.	Transformer resistance (referred to HV side)
R	Ω	Resistance
R’	Ω/m	Distributed resistance
$r_{CU,HV}$	p.u.	Resistance representing copper losses on HV side
$r_{CU,LV}$	p.u.	Resistance representing copper losses on LV side
r_D	p.u.	Resistance of damper winding in d-axis
r_{fd}	p.u.	Field resistance
r_Q	p.u.	Resistance of damper winding in q-axis

r_s	p.u.	Stator resistance
r_{Sc}	p.u.	Transformer short circuit resistance
S_{base}, S_b	MVA	Base apparent power
S_{rated}	MVA	Rated apparent power
S_{Gen}	MVA	Generated apparent power
S_{Sc}	MVA	Short circuit apparent power
S_{Sc}''	MVA	Subtransient short circuit apparent power
S_T	MVA	Transformer apparent power
t_e	p.u.	Electrical torque
t_{off}	s	Circuit breaker closing time
t_{on}	s	Resistor activation time
T_d'	s	Direct axis transient short circuit time constant
T_d''	s	Direct axis subtransient short circuit time constant
T_{d0}'	s	Direct axis transient open loop time constant
T_{d0}''	s	Direct axis subtransient open loop time constant
T_0	Nm	Nominal torque
T_a	Nm	Acceleration torque
T_{act}	s	Resistor on-time
T_e	Nm	Electromagnetic output torque
T_{Gen}	Nm	Generator torque
T_m	Nm	Mechanical torque
T_M	s	Mechanical starting time
T_q''	s	Quadrature axis transient short circuit time constant
T_{q0}''	s	Quadrature axis subtransient open loop time constant
T_{Tur}	Nm	Turbine torque
u	p.u.	Measured generator output voltage
u_1	p.u.	Voltage set point
u_{error}	p.u.	Error signal
u_{fd}	p.u.	Field voltage
u_d	p.u.	Stator voltage in d-axis
u_{Sc}	%	Transformer short circuit voltage
u_q	p.u.	Stator voltage in q-axis
U_0	V	Internal grid voltage
U_G	V	Generator rated voltage
U_{HV}	V	Transformer high voltage
U_{LV}	V	Transformer low voltage
U_{nom}	V	Nominal grid voltage
V_{grid}	V	Grid voltage

v_{PCC}	p.u.	Voltage at PCC during a fault
$v_{PCC,average}$	p.u.	Average remaining voltage at PCC
W_B	-	Specific torque characteristic
W_H	-	Specific turbine characteristic
$x_{\sigma,HV}$	p.u.	Transformer leakage reactance (HV side)
$x_{\sigma,LV}$	p.u.	Transformer leakage reactance (LV side)
x_d	p.u.	Synchronous reactance in d-axis
x_d'	p.u.	Transient reactance in d-axis
x_d''	p.u.	Subtransient reactance in d-axis
$x_{d,sat}''$	p.u.	Subtransient reactance in d-axis saturated
x_{fd}	p.u.	Field reactance
x_{fdD}	p.u.	Reactance representing mutual flux between field and damper (i.e. characteristic reactance)
x_l	p.u.	Stator leakage reactance
$xl_{,sat}$	p.u.	Stator leakage reactance saturated
x_M	p.u.	Transformer magnetizing reactance
x_{md}	p.u.	Main reactance in d-axis
x_{mq}	p.u.	Main reactance in q-axis
x_q	p.u.	Synchronous reactance in q-axis
x_q'	p.u.	Transient reactance in q-axis
x_q''	p.u.	Subtransient reactance in q-axis
x_{rl}	p.u.	Characteristic reactance as denoted in DIgSILENT PowerFactory
x_{Sc}	p.u.	Transformer short circuit reactance
x_T	p.u.	Transfomer reactance (referred to HV side)
x_{fault}	p.u.	Fault reactance
X_{fault}	Ω	Fault reactance
y	p.u.	Guide vane opening
z_{Sc}	p.u.	Transformer short circuit impedance
$Z_{b,HV}$	Ω	Base impedance on HV side
$Z_{b,LV}$	Ω	Base impedance on LV side
Z_{grid}	Ω	Grid impedance

Table of Contents

1 Introduction

1.1 Background

In the past large generating units with high inertia used to secure voltage and frequency stability within the power system almost exclusively, allowing smaller units to disconnect from the grid during voltage sags. Hence, most grid codes did not require smaller and decentralized power plants to support the power system during fault events. In recent years, however, the electric power produced by decentralized power plants such as wind turbines and solar panels increased significantly in many countries. The highly fluctuating in-feed from renewable sources coupled with more dynamic cross-border exchanges between countries as a result of the liberalization of the energy market constitute new challenges to the transmission system operators (TSOs).

TSOs have recognized the need for change and started adapting their grid codes in order to face the newly arisen challenges. To further ensure a high level of security and reliability of the power system, synchronous generating units need to remain stable and connected to the network during and after periods of low grid voltage. This requirement is also known as Low Voltage Ride Through (LVRT) or Fault Ride Through (FRT) capability. Its adherence is particularly important to avoid loss of generation and thus, the collapse of system frequency during and after faults [1].

The European Network of Transmission System Operators for Electricity (ENTSO-E) has released a network code comprising different already existing grid codes across ENTSO-E member countries. It serves as a guideline for TSOs in Europe while it still leaves a high degree of national choice. ENTSO-E's *Network Code for Requirements for Grid Connection Applicable to All Generators* has been extended to all synchronous generators connected to the power system and specifies the required LVRT capability based on a voltage against time profile.

1.2 Goal

Bulb generators driven by horizontal Kaplan turbines are often used in run-of-river power plants due to their high efficiency at low heads of up to 30 meters. Reduced size and cost as well as higher flow capacities are other key benefits compared to solutions with vertical constructions. On the negative side, very low inertia makes bulb generators prone to losing synchronism when subjected to low grid voltages at their connection points.

This thesis is structured into two parts: on the one hand it is examined to what extend hydraulic bulb type generating units fulfill the LVRT requirements as specified by the German as well as the Nordic GCs. The main goal, on the other hand, is to assess the improvement of the generator's FRT capability and hence its stability by means of resistive braking.

1.3 Methods and Tools

The simulations necessary for assessing the LVRT capability of the considered machine are carried out using two different tools: *DIgSILENT Powerfactory* (PF) and *OpenModelica* (OM).

DIgSILENT PowerFactory is an already proven standard in the industry that allows modelling, analysis and simulation of power systems. Generally there are two simulation methods available that enable all transient phenomena in the electrical power system to be analyzed. The RMS (root mean square) simulation uses a steady-state network model for mid-term and long-term transient stability studies taking only the fundamental components of voltages and currents into account. Analysis of short-term transients (i.e. electromagnetic transients) are carried out by running the so-called EMT simulation function which is based on a dynamic network model considering generator flux and stator voltage equations without simplification. Both simulation functions are applicable to networks under balanced as well as unbalanced conditions.

OpenModelica is an open-source simulation environment for Modelica applications, a declarative, object-oriented and equation-based language for modelling and simulating complex dynamic systems. OM is a project supported by the Open Source Modelica Consortium with the goal of providing an interactive computational environment for Modelica for both academic and industrial applications [4]. The Modelica components library used in this work was developed and provided by Andritz Hydro.

The different modelling approaches applied in the two simulators are compared within the scope of this thesis (Chapter 2). How these differences affect the simulation results is analyzed in Chapter 3 using examples of the LVRT study.

.

2 Modelling of network components

The simulations in OpenModelica and PowerFactory are based on two different models. In the following, the modelling approach of the underlying network components is thoroughly described to allow a deeper understanding of the resulting differences in the simulation outcomes. Figure 2-1 gives an overview of the following task.

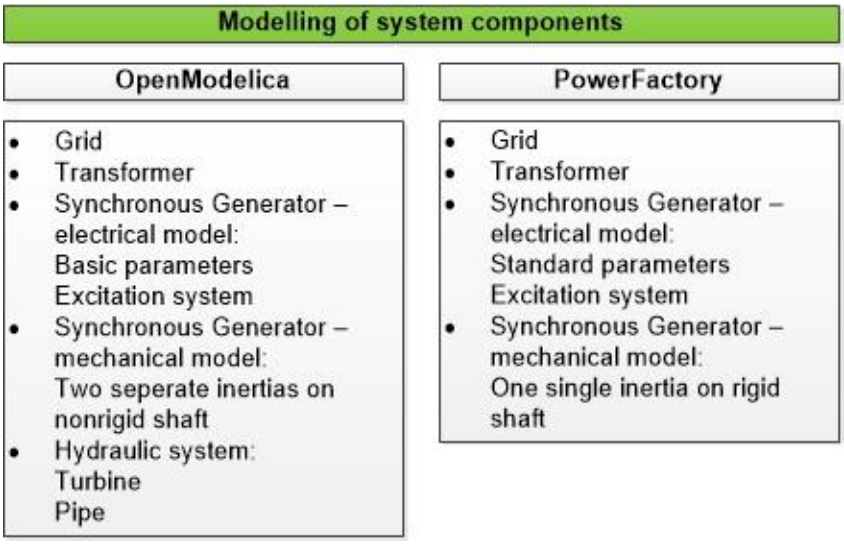

Figure 2-1: System modelling overview

2.1 Synchronous Generator – Electrical Model

Synchronous generators driven by hydraulic turbines rotate at low speeds and thus, require a large number of poles. Therefore, a rotor with salient poles and concentrated windings is used.

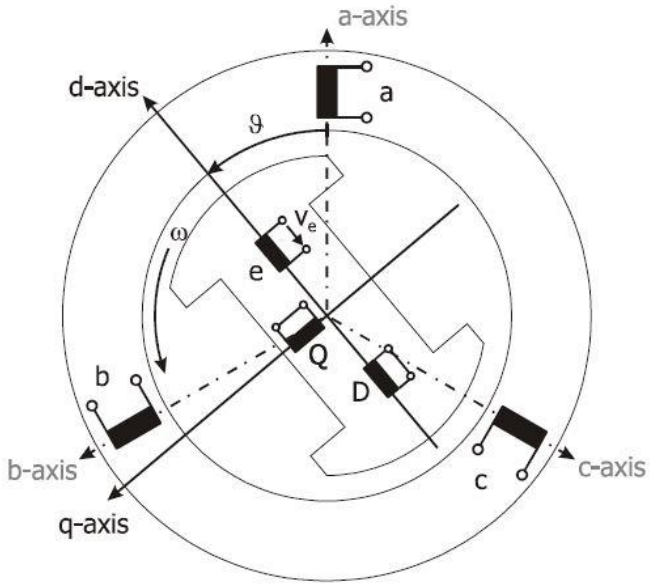

Figure 2-2: Three phase salient rotor synchronous machine [2]

When modelling synchronous machines it is convenient to use the *dq0-transformation*, also known as *Park's Transformation*, where all state variables from the stator reference frame are transformed to a rotating coordinate system with orthogonal d- and q-axes (i.e. direct and quadrature axes) in the rotor

reference frame which is revolving at rotor speed. The d-axis is aligned with the magnetic axis of the excitation winding whereas the q-axis is arbitrarily chosen to lead the d-axis by 90 degrees as depicted in Figure 2-2. The 0-component vanishes under balanced operation [3] [4] [5].

The armature windings in the stator reference frame are indicated by a, b and c in Figure 2-2. D and Q represent the amortisseur circuits in d- and q-axis (i.e. rotor reference frame), respectively. PowerFactory allows the definition of one damper winding for the d-axis and up to two damper windings for the q-axis [2]. The excitation winding 'e' is only considered in the d-axis and will be denoted by 'fd' (i.e. field) in the following. The angle ϑ between the d- and a-axis corresponds to the mechanical rotor angle and increases continuously since the rotor rotates with angular velocity ω_r with respect to the stator. The relationship between the mechanical and the electrical rotor angle is given by the number of poles p:

$$\vartheta_{el} = \frac{p}{2} \cdot \vartheta_m \tag{1}$$

2.1.1 OpenModelica

A highly accurate mathematical model using d- and q-components and completely specifying a synchronous machine's electrical characteristics as used in OpenModelica is derived in the following. All quantities are given in per unit (p.u.).

Stator voltage equations (stator current in generator orientation)

$$u_d = r_s i_d + \frac{1}{\omega_0} \cdot \frac{d\psi_d}{dt} - \omega\psi_q \tag{2}$$

$$u_q = r_s i_q + \frac{1}{\omega_0} \cdot \frac{d\psi_q}{dt} + \omega\psi_d \tag{3}$$

Rotor voltage equations

$$u_{fd} = r_{fd} i_{fd} + \frac{d\psi_{fd}}{\omega_0 dt} \tag{4}$$

$$0 = r_D i_D + \frac{d\psi_D}{\omega_0 dt} \tag{5}$$

$$0 = r_Q i_Q + \frac{d\psi_Q}{\omega_0 dt} \tag{6}$$

Flux linkage equations for d-axis

$$\psi_d = \left(x_l \cdot k_{sat} + x_{md}\right) \cdot i_d + x_{md} \cdot i_{fd} + x_{md} \cdot i_D \tag{7}$$

$$\psi_{fd} = x_{md} \cdot i_d + \left(x_{md} + x_{fdD} + x_{fd}\right) \cdot i_{fd} + \left(x_{md} + x_{fdD}\right) \cdot i_D \tag{8}$$

$$\psi_D = x_{md} \cdot i_d + \left(x_{md} + x_{fdD}\right) \cdot i_{fd} + \left(x_{md} + x_{fdD} + x_D\right) \cdot i_D \tag{9}$$

Flux linkage equations for q-axis

$$\psi_q = \left(x_l \cdot k_{sat} + x_{mq}\right) \cdot i_q + x_{mq} \cdot i_Q \tag{10}$$

$$\psi_Q = x_{mq} \cdot i_q + \left(x_{mq} + x_{fdD} + x_Q\right) \cdot i_Q \tag{11}$$

Electrical torque t_e

$$t_e = \psi_d i_q - \psi_q i_d \tag{12}$$

The currents in the armature and field windings are constant during steady-state operation while there is no current flowing through the damper windings. Hence, the flux will also remain constant. In this case the synchronous reactance is acting:

$$x_d = x_{md} + x_l \tag{13}$$

$$x_q = x_{mq} + x_l \tag{14}$$

From equations (7) and (10) it can be observed that the generator model in OpenModelica takes the saturation of the stator leakage reactance into consideration. The saturation factor k_{sat} determines the effective reactance as seen from the machine's terminal as a function of the stator current. During steady-state conditions k_{sat} equals 1 and declines with increasing stator current.

The reactance x_{fdD} represents the mutual flux between field and damper windings allowing a better approximation of the field current during transient events. The parameter is assumed to be zero throughout this thesis.

The equations above describe the synchronous machine characteristics using the so-called *basic* or *fundamental parameters* which refer to the reactances and resistances of the stator and rotor circuits. They cannot be determined from measured responses of the machine. The more common approach as applied in PowerFactory is to derive the parameters from observed behavior during short-circuit and open-loop tests, also known as *standard parameters*. The relationship between fundamental and standard parameters is given in the next section.

2.1.2 PowerFactory

Faults in the electrical system, such as short circuits, cause transient phenomena which result in variations of the flux components. Hence, it is not justified to assume steady-state parameters. During the initial cycles the amplitude of the short circuit current decays very rapidly which is also referred to as *subtransient period*. To characterize the associated changes in magnetic flux, the subtransient reactances x_d'' and x_q'' become effective which also include the impact of the damper windings.

$$x_d'' = x_d \cdot \frac{T_d' \cdot T_d''}{T_{d0}' \cdot T_{d0}''} = x_l + \frac{x_D \cdot x_{fd} \cdot x_{md} + x_D \cdot x_{fdD} \cdot x_{md} + x_{fdD} \cdot x_{fd} \cdot x_{md}}{x_{md} \cdot x_{fd} + x_{md} \cdot x_D + x_D \cdot x_{fd} + x_D \cdot x_{fdD} + x_{fd} \cdot x_{fdD}} \tag{15}$$

$$x_q'' = x_q \cdot \frac{T_q''}{T_{q0}''} = x_l + \frac{x_{mq} \cdot x_Q}{x_{mq} + x_Q} \tag{16}$$

The transient reactance for periods during which the amplitude decays more slowly before reaching steady-state conditions is given by:

$$x_d^{'} = x_d \cdot \frac{T_d^{'}}{T_d^{''}} = x_l + \frac{x_{md} \cdot \left(x_{fd} + x_{fdD}\right)}{x_{md} + x_{fd} + x_{fdD}} \tag{17}$$

The q-axis of a salient pole machine contains only one rotor circuit representing subtransient effects. No distinction is made between transient and synchronous (steady-state) conditions. Thus, x_q' and T_{q0}' are not applicable.

The duration of the subtransient and transient time intervals are given by the short-circuit time constants T_d' and T_d'' as well as the open-loop time constants T_{d0}' and T_{d0}''. They are defined for the q-axis in a similar way. In this thesis the "classical expressions" according to Prabha Kundur are applied which are based on the assumptions that the field resistance r_{fd} is equal to zero and that $r_D \rightarrow \infty$ during subtransient and transient periods, respectively [3].

Short-circuit time constants in seconds

$$T_d^{'} = \frac{1}{\omega_0 \cdot r_{fd}} \cdot \left(x_{fd} + x_{fdD} + \frac{x_{md} \cdot x_l}{x_{md} + x_l} \right) \tag{18}$$

$$T_d^{''} = \frac{1}{\omega_0 \cdot r_D} \cdot \left(x_D + \frac{x_{md} \cdot x_{fdD} \cdot x_{fd} + x_{md} \cdot x_{fd} \cdot x_l + x_l \cdot x_{fdD} \cdot x_{fd}}{x_{fd} \cdot x_{md} + x_{fd} \cdot x_l + x_{fdD} \cdot x_{md} + x_{fdD} \cdot x_l + x_l \cdot x_{md}} \right) \tag{19}$$

$$T_q^{''} = \frac{1}{\omega_0 \cdot r_Q} \cdot \left(x_Q + \frac{x_{mq} \cdot x_l}{x_{mq} + x_l} \right) \tag{20}$$

Open-loop time constants in seconds

$$T_{d0}^{'} = \frac{1}{\omega_0 \cdot r_{fd}} \cdot \left(x_{md} + x_{fd} + x_{fdD} \right) \tag{21}$$

$$T_{d0}^{''} = \frac{1}{\omega_0 \cdot r_D} \cdot \left(x_D + \frac{x_{fd} \cdot \left(x_{md} + x_{fdD} \right)}{x_{fdD} + x_{fd} + x_{md}} \right) \tag{22}$$

$$T_{q0}^{''} = \frac{1}{\omega_0 \cdot r_Q} \cdot \left(x_Q + x_{mq} \right) \tag{23}$$

The derived standard parameters are further simplified by omitting the characteristic reactance x_{fdD} (denoted in PowerFactory by x_{fl}).

PowerFactory offers a sixth order generator model for RMS-simulations which neglects the stator flux transients ($\frac{d\psi_d}{dt} = \frac{d\psi_q}{dt} = 0$, $\omega\dot{\psi}_d \approx \dot{\psi}_d$ and $\omega\dot{\psi}_q \approx \dot{\psi}_q$) and reduces the equations (2) and (3) to:

$$u_d = r_s \cdot i_d - x_q^{''} \cdot i_q + u_d^{''} = r_s \cdot i_d - x_q^{''} \cdot i_q - \psi_q^{''} \tag{24}$$

$$u_q = r_s \cdot i_q - x_d^{''} \cdot i_d + u_q^{''} = r_s \cdot i_q - x_d^{''} \cdot i_d + \psi_d^{''} \quad (25)$$

PowerFactory does provide means to model saturation effects. However, these are limited to the mutual reactances x_{md} and x_{mq}. High currents after faults on the network, such as short-circuits, will lead to a saturation of the leakage reactance x_l. Disregarding this effect might cause an underestimation of the short circuit currents.

The available generator data of the examined machine gives only values on the saturation of the stator leakage reactance and the subtransient reactance x_d'' which is not included in PowerFactory's model. In order to include the saturation effects, the saturated values for x_l and x_d'' are chosen as input parameters in PowerFactory. This is a justified assumption since there are no changes observed during steady-state operation when using saturated values instead of unsaturated. For non-critical clearing times by contrast, the influence of a lower x_d'' value is evident during both subtransient and transient periods where damping is slightly increased as depicted in Figure 2-3. Saturation effects are more obvious in the rotor angle displacement for critical fault clearing times.

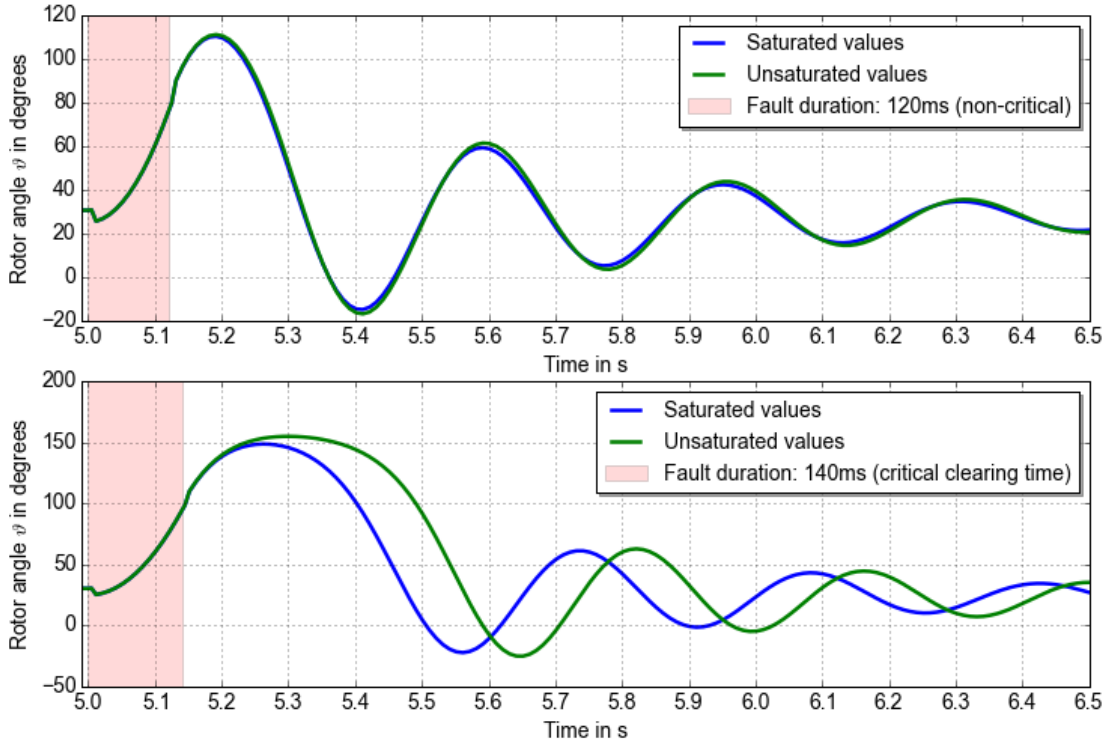

Figure 2-3: Saturation effects on rotor angle excursions

The RMS-simulation requires the following input data: x_d'', x_d', x_d, x_l, x_{rl}, T_d'', T_d', x_q'', x_q and T_q''. All other required parameters, such as x_{fd}, r_{fd}, x_D, x_Q, r_D and r_Q are computed and modelled internally.

2.2 Synchronous Generator – Mechanics

2.2.1 General

An acceleration or deceleration of the rotor is caused by an unbalance between mechanical input torque T_m and electromagnetic output torque T_e. Therefore, it is of utmost importance to include a synchronous generator's equations of motion in power system stability studies to describe the machine's mechanical characteristics.

The combined inertia of the generator and turbine J is accelerated by an unbalance in torques:

$$\frac{J \cdot \omega_0^2}{p^2 \cdot S_{base}} \cdot \frac{d\omega}{dt} = T_m - T_e = T_a \tag{26}$$

When using a very detailed electrical model of the generator, the power provided by the damping windings is already included in the electrical power and hence, in the electrical torque T_e of eq. (26). That is why an explicit term for the damping is not considered [6].

The difference between the actual angular velocity of the rotor and its rated value in electrical rad/s yields the time derivative of the rotor's angular position ϑ:

$$\frac{d\vartheta}{dt} = \omega - \omega_0 = \Delta\omega \tag{27}$$

The inertia of the generator and the turbine is often expressed as the inertia time constant H in s based on the rated apparent power:

$$H = \frac{1}{2} \cdot \frac{J \cdot \omega_0^2}{p^2 \cdot S_{rated}} \tag{28}$$

The mechanical starting time or acceleration time constant required for rated torque to accelerate the rotor from standstill to rated speed is given by:

$$T_M = 2H \tag{29}$$

H and T_M can be entered in PowerFactory based on S_{rated} or P_{rated} and contain the information of the combined inertia of generator, turbine and water in case of hydraulic units. The mechanical system composed of turbine and generator is assumed to be one rotating mass on a rigid shaft. The turbine delivers constant mechanical input power which is justified during subtransient periods after a fault where the turbine governor has not yet reacted to the change in electrical output power. Especially hydraulic turbine governors have a very slow response from a viewpoint of transient stability allowing their influence to be neglected. The tool offers no possibility to model the mechanical and hydraulic components of the hydroelectric power plant more accurately.

2.2.2 Modelling of mechanical and hydraulic components in OpenModelica

Modelica is as an equation based language enabling to model any kind of physical system. Therefore, the model used in OpenModelica contains a much more detailed approximation of the mechanical as well as hydraulic subcomponents.

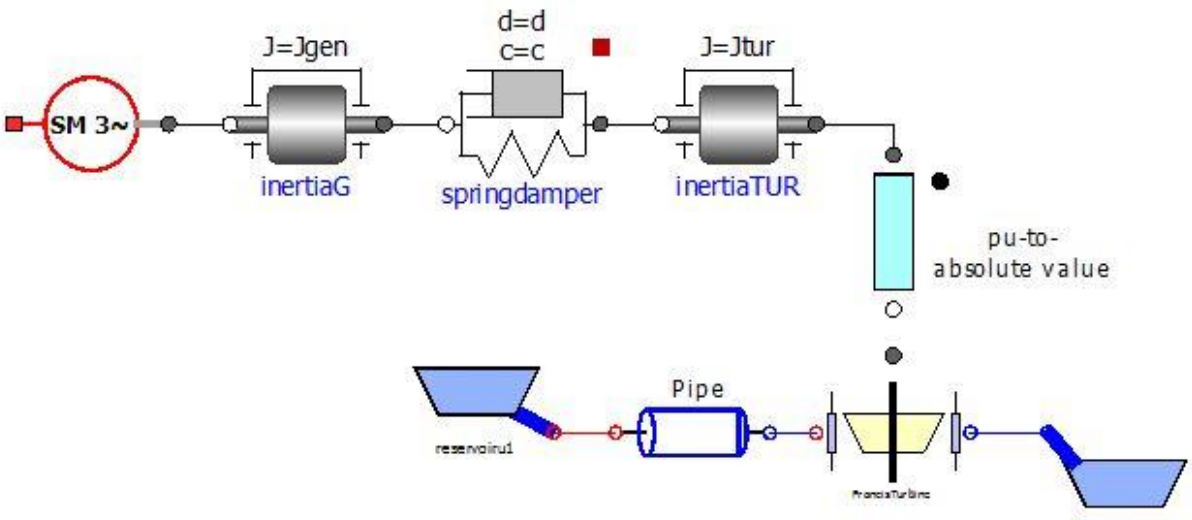

Figure 2-4: Mechanical and hydraulic components in OpenModelica

Figure 2-4 shows one part of the examined system. The electrical model of the generator has been discussed in chapter 2.1 and is indicated by the red icon (SM 3~). This component does not merely include the model based on fundamental components but also encompasses the generator's excitation system which is briefly discussed in chapter 2.3.

The drive train is represented with a two-mass shaft model. The inertias of generator and turbine are considered separately and connected via a spring-damper representing the elasticity and mechanical damping of the shaft. Thereby possible oscillations between the single components mounted on the shaft are taken into account.

$$\omega = \frac{d\vartheta}{dt} \rightarrow \dot{\omega} = \frac{d^2\vartheta}{dt^2} \tag{30}$$

$$T_{Tur} = J_{Tur} \cdot \frac{d\omega_{Tur}}{dt} + d \cdot \left(\omega_{Tur} - \omega_{Gen}\right) + K \cdot \left(\vartheta_{Tur} - \vartheta_{Gen}\right) \tag{31}$$

$$-T_{Gen} = J_{Gen} \cdot \frac{d\omega_{Gen}}{dt} + d \cdot \left(\omega_{Gen} - \omega_{Tur}\right) + K \cdot \left(\vartheta_{Gen} - \vartheta_{Tur}\right) \tag{32}$$

The Kaplan turbine and the penstock are modelled very accurately including their dynamic behaviors according to Christophe Nicolet's modelling approach described in his thesis "Hydroacoustic Modelling and Numerical Simulation of unsteady Operation of hydroelectric Systems" [7].

The dynamic behavior of an elementary pipe of length dx is characterized by a set of differential equations, namely the equation of motion and the equation of continuity:

$$\begin{cases} \dfrac{\partial h}{\partial x} + \dfrac{1}{g \cdot A} \cdot \dfrac{\partial Q}{\partial t} + \dfrac{\lambda \cdot Q \cdot |Q|}{2 \cdot g \cdot D \cdot A^2} = 0 \\ \dfrac{\partial h}{\partial t} + \dfrac{a^2}{g \cdot A} \cdot \dfrac{\partial Q}{\partial x} = 0 \end{cases} \tag{33}$$

It can be observed that there is a striking similarity between the modelling of the propagation of pressure waves in hydraulic systems (eq. (33)) and the so-called “telegrapher’s equations” describing the voltage and current propagation in a conductor with respect to time and distance.

$$\begin{cases} \dfrac{\partial U}{\partial x} + L_e^{'} \cdot \dfrac{\partial i}{\partial t} + R_e^{'} \cdot i = 0 \\ \dfrac{\partial U}{\partial t} + \dfrac{1}{C_e^{'}} \cdot \dfrac{\partial i}{\partial x} = 0 \end{cases} \tag{34} \quad \longleftrightarrow \quad \begin{cases} \dfrac{\partial h}{\partial x} + L^{'} \cdot \dfrac{\partial Q}{\partial t} + R^{'}(Q) \cdot Q = 0 \\ \dfrac{\partial h}{\partial t} + \dfrac{1}{C^{'}} \cdot \dfrac{\partial Q}{\partial x} = 0 \end{cases} \tag{35}$$

Both systems have two state variables: discharge Q and current i as well as head h and voltage V. The two sets of equation (34) and (35) show that it is possible to define distributed as well as lumped hydracoustic parameters analogous to their electrical counterparts:

$$R^{'} = \frac{\lambda \cdot |Q|}{2 \cdot g \cdot D \cdot A^2} \left[s/m^3 \right] \leftrightarrow R = \frac{\lambda \cdot |Q|}{2 \cdot g \cdot D \cdot A^2} \cdot \frac{l}{n} \left[s/m^2 \right] \tag{36}$$

$$L^{'} = \frac{1}{g \cdot A} \left[s^2/m^3 \right] \leftrightarrow L = \frac{1}{g \cdot A} \cdot \frac{l}{n} \left[s^2/m^2 \right] \tag{37}$$

$$C^{'} = \frac{g \cdot A}{a^2} [m] \leftrightarrow C = \frac{g \cdot A}{a^2} \cdot \frac{l}{n} \left[m^2 \right] \tag{38}$$

With:

A: pipe cross-section [m^2]

Q: discharge [m^3/s]

g: gravitational acceleration [m/s^2]

a: wave speed [m/s]

D: pipe diameter [m]

λ: local loss coefficient [-]

l: length of pipe [m]

n: number of segments [-]

With the information above the pipe can be modelled using an equivalent electrical circuit composed of two resistances, two inductances and one capacitance as shown in Figure 2-5.

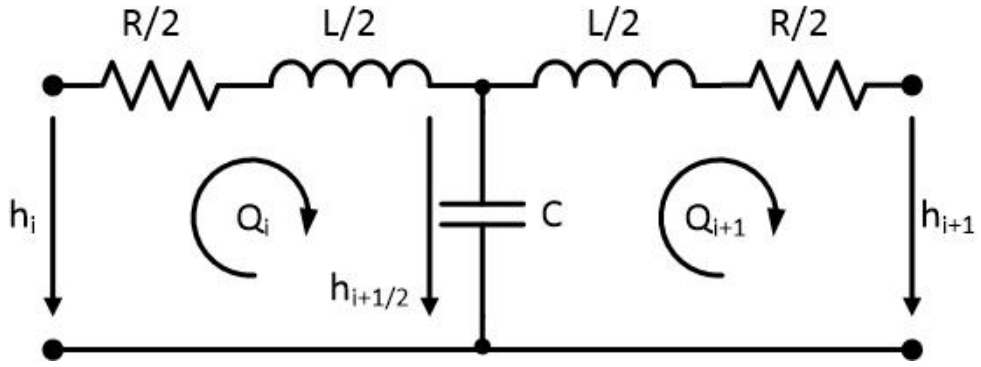

Figure 2-5: Equivalent scheme of a pipe

The hydroacoustic inductance, capacitance and resistance represent the inertia effect of the water, the storage effect due to the pressure increase and the head losses through the pipe, respectively.

A full-length pipe is represented by n segments:

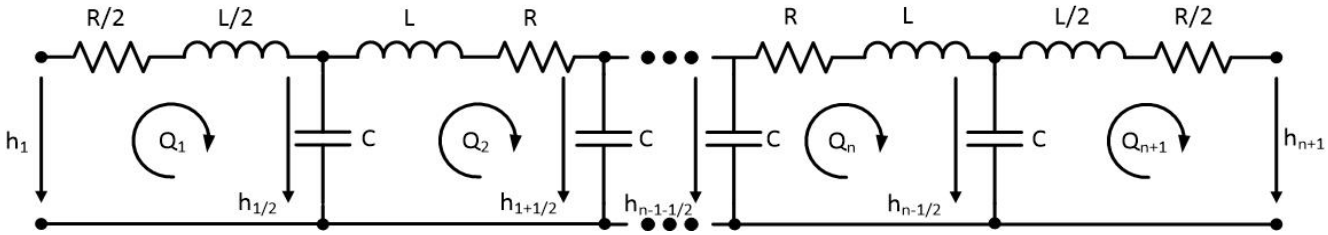

Figure 2-6: Equivalent scheme of a full length pipe with n segments

The equations implemented in OpenModelica describing the relationship between the two hydraulic state variables, discharge q and head h, are based on the laws from electric circuit theory:

$$h = R \cdot q \tag{39}$$

$$h = L \cdot \frac{dq}{dt} \tag{40}$$

$$q = C \cdot \frac{dh}{dt} \tag{41}$$

Due to the complexity of modelling the transient behavior of hydraulic machines, the “quasi-static” approach is applied to reconstruct the turbine. Hereby, it is assumed that during transient events the machine experiences a series of different steady-state operating points which are characterized by the energy E (=g*h), the discharge Q, the rotational speed N, the torque T and the guide vane opening y. The turbine converts hydraulic power P_h to mechanical power P_m with the highest hydraulic efficiency η_h.

$$P_h = \rho \cdot Q \cdot E = \rho \cdot g \cdot Q \cdot h \tag{42}$$

$$P_m = \omega \cdot T \tag{43}$$

$$\eta_h = \frac{P_m}{P_h} = \frac{\omega \cdot T}{\rho \cdot g \cdot Q \cdot h} \tag{44}$$

The Kaplan turbine representation is based on Christoph Nicolet's Francis turbine model with adjustable guide vanes. However, Kaplan turbines are equipped with both adjustable guide as well as adjustable runner vanes allowing an optimization of the water's angle of attack and thus increasing the hydraulic efficiency. As a consequence, Kaplan turbines have the blade pitch angle as an additional parameter compared to such of Francis type. Guide and runner vanes are assumed to be fixed during operation since there are no notable changes when a fault of a few milliseconds occurs, allowing the Francis model to be used.

For the quasi-static approach, the turbine features are defined in a polar coordinate system where the specific turbine characteristic W_H and the specific torque characteristic W_B are represented as a function of the polar angle Θ and the guide vane opening y as depicted in Figure 2-7.

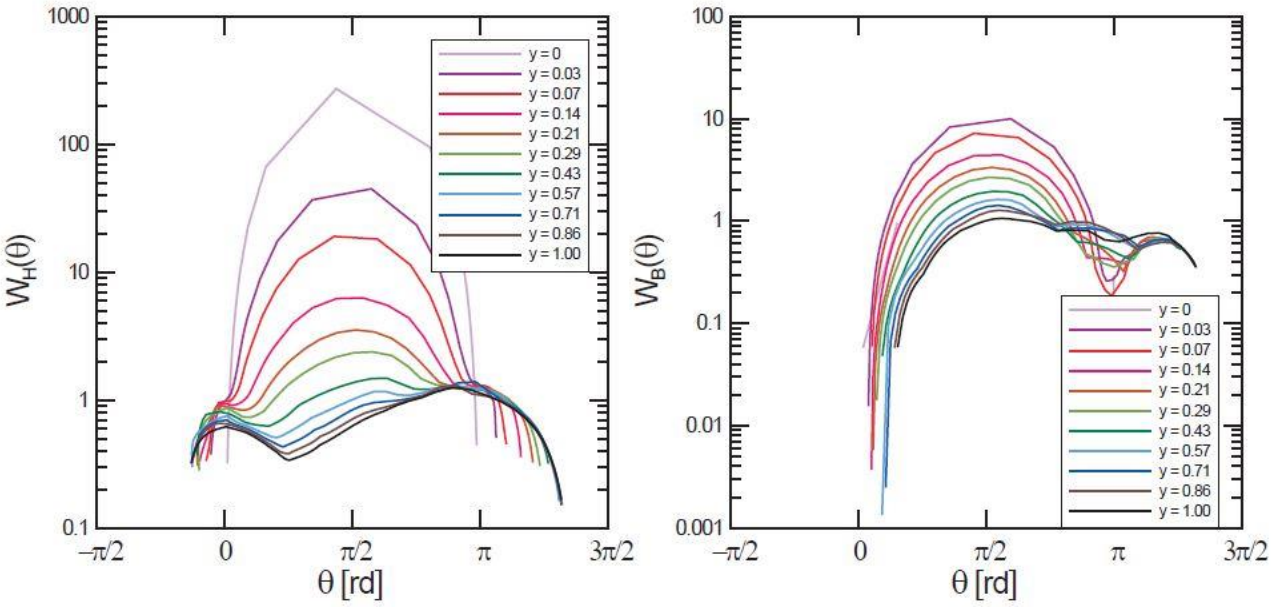

Figure 2-7: Polar representation of turbine characteristics [5]

The characteristic functions and the polar angle are given by:

$$\Theta = \arctan\left(\frac{Q/Q_0}{N/N_0}\right) \tag{45}$$

$$W_H(\Theta) = \frac{H/H_0}{\left(Q/Q_0\right)^2 + \left(N/N_0\right)^2} \tag{46}$$

$$W_B(\Theta) = \frac{T/T_0}{\left(Q/Q_0\right)^2 + \left(N/N_0\right)^2} \tag{47}$$

The index 0 refers to nominal values.

Rearranging equations (46) and (47) yields the effective head and effective output torque at the operating point. The model in OpenModelica is provided with a table containing typical W_H and W_B values for corresponding angles Θ which are calculated using equation (45).

2.3 Excitation System

Excitation systems are used to control the output of a generator by adjusting the input voltage which is proportional to the direct current supplied to the machine field winding. Simultaneously, the excitation system controls reactive power flows contributing to the enhancement of system stability [3]. Figure 2-8 shows the block diagram of the system used for both models.

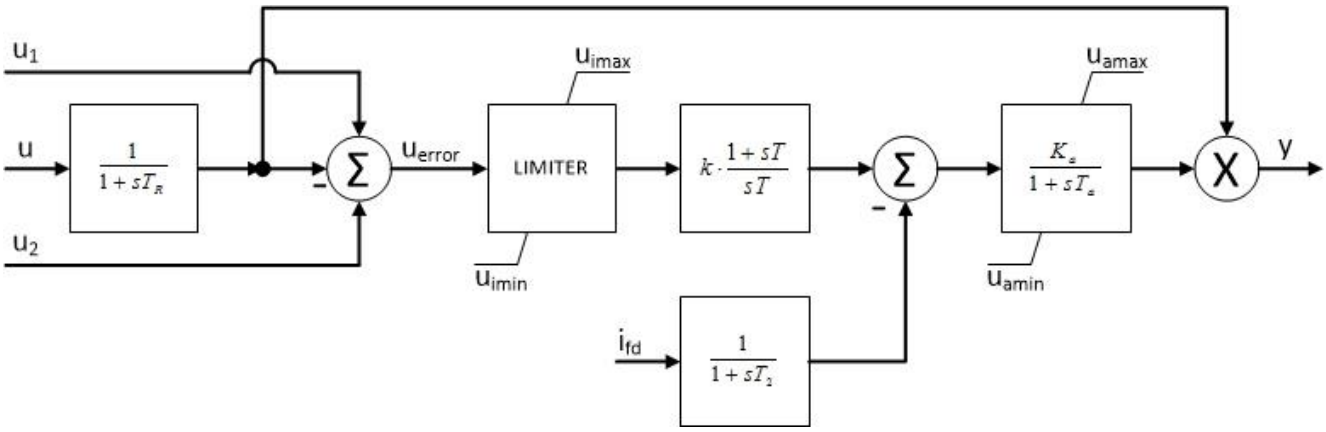

Figure 2-8: Excitation system

At the summing point of the AVR a voltage set point u_1 is compared to the measured generator output voltage u. Provision is made for an additional error signal u_2 from a Power System Stabilizer. The time delays due to measuring, rectifying and filtering signals are characterized by transducers (first order transfer function) with time constants T_R and T_2 for processing stator voltage and field current, respectively.

The comparison between u and u_1 produces an error signal which determines the firing angle for the rectifiers and is zero during steady-state operation when the generator output voltage is equal to the reference voltage. The error signal is bounded and supplied to a proportional-integral controller which is integrated in the forward path of control systems to reduce the steady-state errors.

K_a and T_a represent the voltage regulator gain and the exciter's time constant while the field voltage limits are termed u_{amax} and u_{amin}. Among others, the value of K_a determines the damping of electromechanical oscillations [5].

The output y corresponds to the exciter output voltage V_{ex} (i.e. U_{fd}) and is further fed to a block that computes the product of its input with a gain according to equation (48). The generator field voltage u_{fd} in p.u. that is supplied to the field windings is determined by the generator equations.

$$u_{fd} = \frac{r_{fd}}{x_{md}} \cdot V_{ex} \tag{48}$$

The AVR reference is given by equation (49) and takes a value corresponding to the generator loading condition prior to the fault [3].

$$u_1 = u_{set} = \frac{V_{ex}}{K_a} + u \tag{49}$$

2.4 Transformer

2.4.1 DIgSILENT PowerFactory [8]

The RMS simulation uses a very detailed transformer model that includes all shunt and branch impedances as shown in the figure below. Given that only balanced, three-phase faults are simulated, it is enough to focus on the positive sequence model.

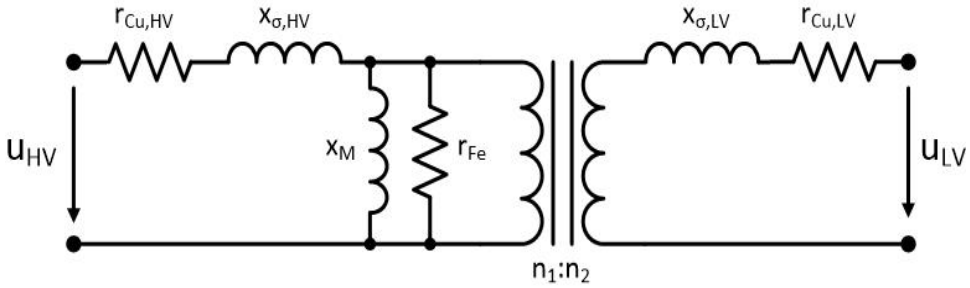

Figure 2-9: Positive sequence model of two-winding transformer (p.u.)

The p.u. values are calculated based on the high-voltage or low-voltage base impedance:

$$Z_{b,HV} = \frac{(U_{b,HV})^2}{S_b} \tag{50}$$

$$Z_{b,LV} = \frac{(U_{b,LV})^2}{S_b} \tag{51}$$

The leakage reactances and winding resistances are obtained from the short-circuit impedance.

$$z_{Sc} = \frac{u_{sc}}{100} \tag{52}$$

$$r_{Sc} = \frac{P_{Cu}/1000}{S_T} \tag{53}$$

$$x_{Sc} = \sqrt{z_{Sc}^2 - r_{Sc}^2} \tag{54}$$

$$r_{Cu,HV} = \gamma_{R,HV} \cdot r_{Sc} \tag{55}$$

$$r_{Cu,LV} = (1 - \gamma_{R,HV}) \cdot r_{Sc} \tag{56}$$

$$x_{\sigma,HV} = \gamma_{X,HV} \cdot x_{Sc} \tag{57}$$

$$x_{\sigma,LV} = (1 - \gamma_{X,HV}) \cdot x_{Sc} \tag{58}$$

Since there is no data available on the iron core losses, they are assumed to be zero and the shunt branch consists only of the magnetizing reactance that can be obtained from the no-load current:

$$x_M = \frac{1}{i_0/100} \tag{59}$$

2.4.2 OpenModelica

The magnetizing branch in Figure 2-9 representing the core losses is often neglected in power system studies because the shunt current is insignificantly small compared to the load current. The replacing elements r_T and x_T are referred to the transformer's primary side (i.e. high voltage side) and obtained from its apparent power, the short-circuit voltage and the copper losses [9]. The transformer turns ratio is assumed to be 1.

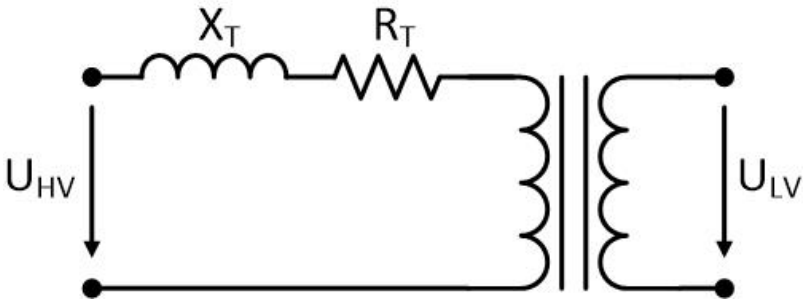

Figure 2-10: Simplified transformer model

$$r_T = \frac{P_{Cu} \cdot \left(U_{b,HV}\right)^2 / S_T^2}{Z_{b,HV}} = P_{Cu} \cdot \frac{S_b}{S_T^2} \tag{60}$$

$$x_T = \frac{u_{Sc} \cdot \left(U_{b,HV}\right)^2 / S_T}{Z_{b,HV}} = u_{Sc} \cdot \frac{S_b}{S_T} \tag{61}$$

2.5 Grid

2.5.1 DIgSILENT Power Factory [10]

The external grid is chosen to be the slack bus controlling the voltage, the angle and the frequency of the bus bar to which it is connected. The power plant is linked via a transformer to a high voltage transmission grid.

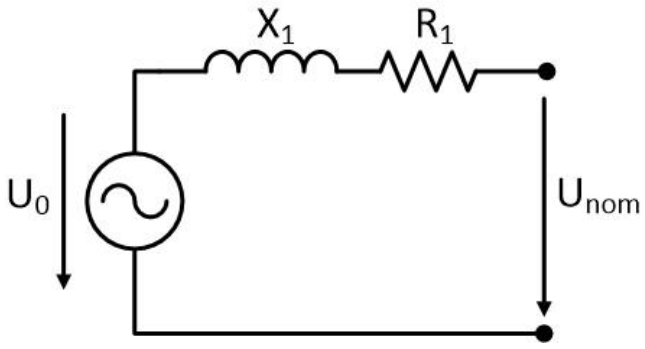

Figure 2-11: Positive sequence model of the external grid

The impedance of the grid is calculated using its short circuit power and assuming a very low ratio between the grid resistance and reactance (R/X = 0,1). The voltage factor c originating from short circuit analysis, is not considered in OM and thus set to 1 in PF to avoid undesired discrepancies between the two models.

$$X_1 = \frac{c}{\sqrt{1+\left(\frac{R}{X}\right)^2}} \cdot \frac{U_{nom}^2}{S_k''} \tag{62}$$

$$R_1 = \frac{R}{X} \cdot X_1 \tag{61}$$

$$U_0 = c \cdot U_{nom} \tag{62}$$

2.5.2 OpenModelica

The grid is modelled via a constant voltage source that takes specific voltage-versus-time profiles as input parameters from a txt-file. The grid impedance is purely reactive since its resistive component is negligibly small in high voltage transmission grids.

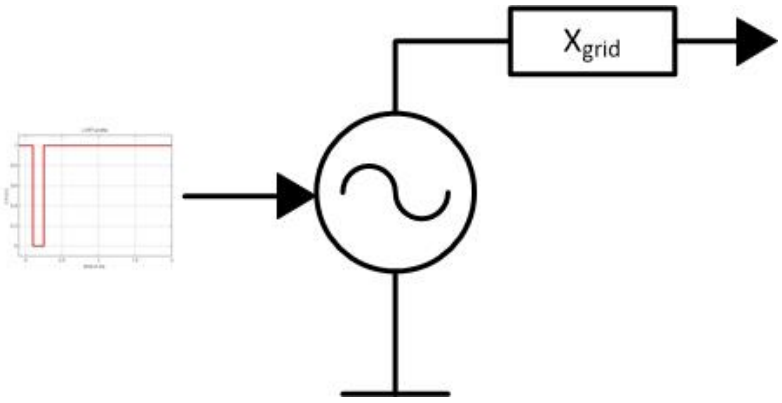

Figure 2-12: External grid modelled with Modelica

The output is constantly 1 p.u. unless a fault is simulated with a corresponding voltage sag. Its magnitude depends among others on the distance between the fault and the recorded location, the impedance of the lines and cables, the connection type of the transformers and the short circuit impedance of the network [11]. By using predefined voltage-against-time profiles, samples from the LVRT envelope curve of the considered grid code can be tested on the system to examine its stability and grid code compliance.

3 Evaluation of grid code compatibility

This chapter deals with the differences between OM and PF regarding their simulation setups and results.

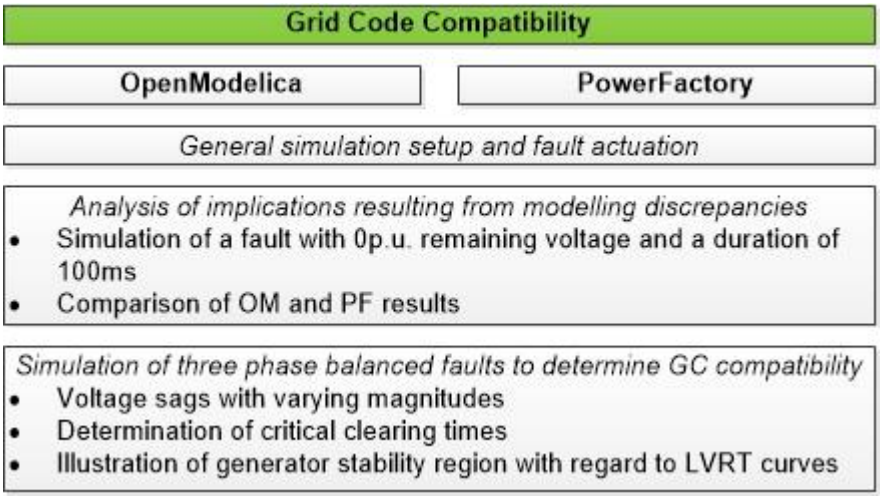

Figure 3-1: Process to determine GC compatibility

3.1 Review of grid codes and grid code requirements

Grid codes are technical specifications which define the requirements that have to be met by power generating facilities connected to a public electrical network. Their main purpose is to ensure safe, secure and reliable supply of energy at minimum cost and with minimum ecological impact. The *quality of power supply* is mainly determined by the constancy of frequency and voltage which is often challenged in the event of small or large disturbances [3]. Faults in the electrical network, such as short circuits or sudden changes in load or generation, causing widespread voltage depressions might under unfavorable circumstances lead to the loss of synchronism of the interconnected synchronous machines. The ability of the generators to remain “in step” after severe transient disturbances is called *transient stability* which highly depends on the pre-fault conditions as well as the duration and severity of the fault.

The capability of generators to *ride through* periods of low grid voltage is an indispensable requirement to ensure power system transient stability. In the past, this grid code specification was almost exclusively limited to large generating units whereas small and decentralized power plants did not need to support the system during grid disturbances [12]. However, the increasing share of renewable energy sources has spurred European TSOs to extend the requirements to all synchronous generating units in order to avoid the loss of a considerable amount of production.

LVRT requirements are defined via voltage-against-time profiles at the connection point where the generating unit is connected to a transmission or distribution grid [13]. The profile describes the conditions on which the generator shall stay connected to the network and continue stable operation [14]. Most grid codes define requirements for balanced faults even though the majority of grid faults is unbalanced. This is based on the assumption that balanced faults have

more severe implications regarding generator stability. Examples of LVRT capability curves from various grid codes are depicted in Figure 3-2.

Voltage sags are sudden changes in RMS voltage to values below 90% of the reference voltage (in transmission grids usually the nominal value). They are mainly characterized by the residual voltage and the duration of the sag [15]. Voltage sags are characterized by most TSOs as either a rectangular or a polygonal curve. The German and Scandinavian grid codes belong to the polygonal voltage sag category whereas the Irish one follows a rectangular pattern.

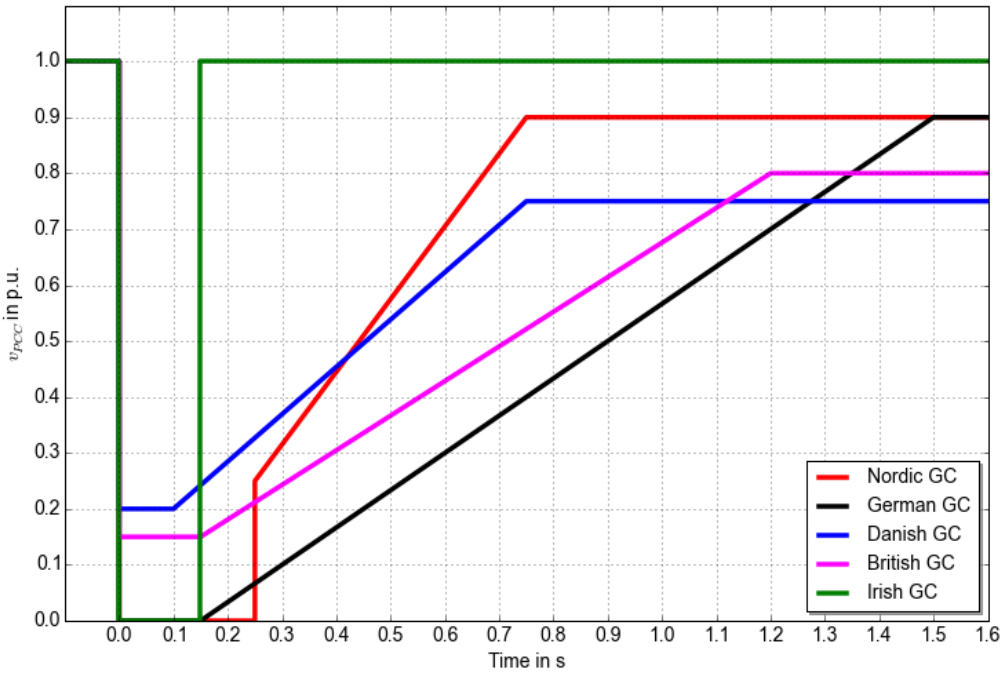

Figure 3-2: Comparison of LVRT requirements

How these voltage profiles are to be interpreted is not evident, though. It can be seen either as an exact voltage-against-time profile at the connection point or as data pairs of voltage sag depth and duration [14].

Yet, studies have shown that the voltage recovers almost instantly after fault clearance. The ability of a generator to remain in synchronism is very much influenced by the voltage return curve. Polygonal shapes with a low gradient are very demanding and might cause tripping of the machine regardless of other conditions supporting system stability [16]. The interpretation as data pairs is considered to be more realistic and recommended by several authors [14] [16] [17] [18] [19]. Hence, in this thesis polygonal curves are seen as an envelope curve comprising all possible faults with rectangular shape within its enclosed area.

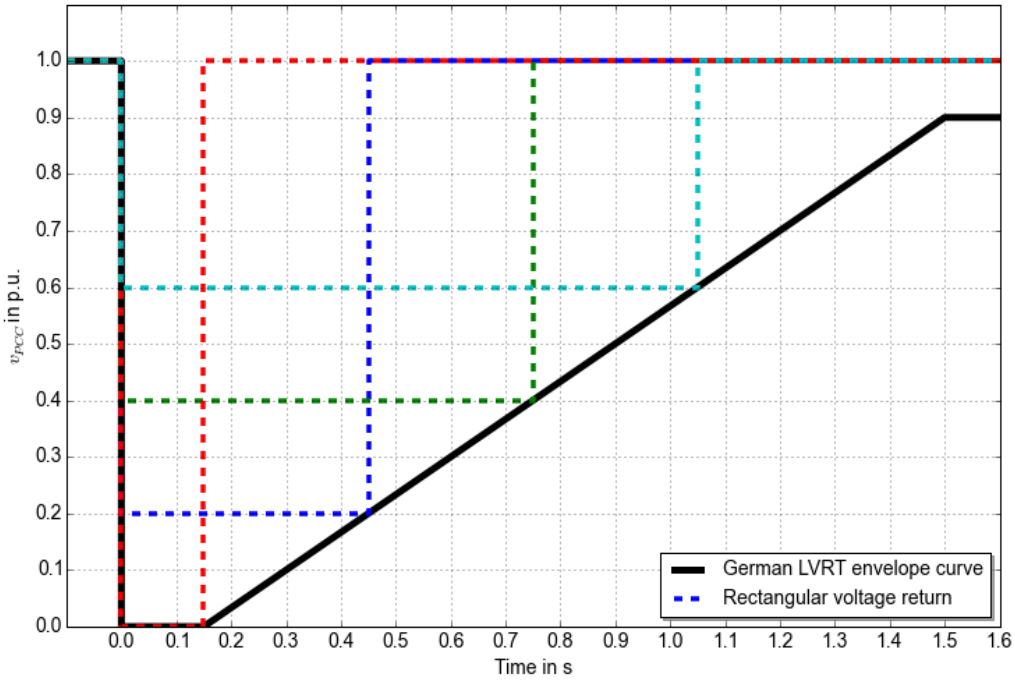

Figure 3-3: Interpretation of rectangular voltage return

Another important parameter that describes voltage sags but has not been included in standards yet constitutes the change in phase angle. During a voltage depression the effective X/R ratio varies bringing about a shift in zero crossing of the instantaneous voltage. However, in this thesis only symmetrical three phase faults are addressed that are characterized by an equal change in magnitude in all phases. A study published in the *International Journal of Scientific Engineering and Technology* demonstrates that there is no significant change in phase angle to be observed for the above-mentioned type of faults [20].

Considering the vast number of grid codes across the EU, the ENTSO-E has undertaken harmonization efforts by proposing a pilot code encompassing requirements from various already existing grid codes. The drawback for simulation purposes of the ENTSO-E Network Code is that it leaves a high degree of interpretation and national choice [13]. Therefore, the German Transmission Code as well as the Nordic Grid Code which clearly define the limits of their LVRT capability curves are taken as a reference in a first approach [21] [22].

3.2 General setup

The machine is exposed to various balanced faults (three phase short circuits) for assessing its grid code compliance and fault response. This section gives an overview of the general simulation setup and the most important data.

The differences in modelling the single components have been thoroughly discussed in chapter 2. Figure 3-4 represents the basic system under test as used in OpenModelica as well as in PowerFactory.

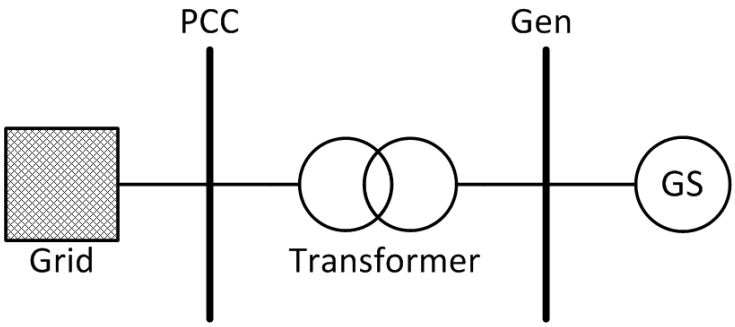

Figure 3-4: General system setup

The external high voltage grid is connected to a bus bar commonly known as *Point of Common Coupling* (PCC) which is chosen to be the slack bus. The generator's output voltage is adjusted to the transmission voltage level of 110 kV using a transformer.

The following table contains the transformer data. Its impedance in the equivalent circuit diagram is represented by x_T and r_T which are calculated using equations (60) and (61).

Table 1: Transformer data

given						calculated	
S_T	U_{HV}	U_{LV}	u_{Sc}	P_{Cu}	i_0	x_T	r_T
MVA	kV	kV	%	kW	%	p.u.	p.u.
24	110	9	13,84	66,67	0,063	0,1528	$3{,}0671*10^{-3}$

The tap changer of the transformer is assumed to be in position 3 (see appendix, Figure 7-1) yielding a voltage and turns ratio of approximately 110kV/9kV.

In this thesis all per unit values are referred to a common MVA base (namely generator rated MVA) regardless of the actual bases applied in OpenModelica and PowerFactory.

Table 2 contains the basic and standard parameters whose relationship is determined by the equations in Chapter 2.1.2.

Table 2: Generator data

Basic parameters		Standard Parameters	
S_G	26,5 MVA	x_d	1,132 p.u.
cos(φ)	0,9 over-exc.	x_q	0,746 p.u.
U_G	9 kV	x_d'	0,444 p.u.
x_{md}	0,94 p.u.	x_d''	0373 p.u.
x_{mq}	0,554 p.u.	x_q''	0,414 p.u.
x_l	0,1942 p.u.	T_d'	1,337 s
r_S	0,0074 p.u.	T_d''	0,038 s
x_D	0,6317 p.u.	T_q''	0,039s
x_Q	0,3695 p.u.	T_{d0}'	3,407 s

r_D	0,0625 p.u.	T_{d0}''	0,045 s
r_Q	0,0419 p.u.	T_{q0}''	0,07 s
r_{fd}	0,0012 p.u.		
x_{fd}	0,3444 p.u.		
x_{fdD}	0 p.u.		

As already indicated, the saturation of the stator leakage reactance is taken into account by considering a saturation factor k_{sat} in the stator flux linkage equations (7) and (10). Its value depends on the generator current and decreases with increasing current.

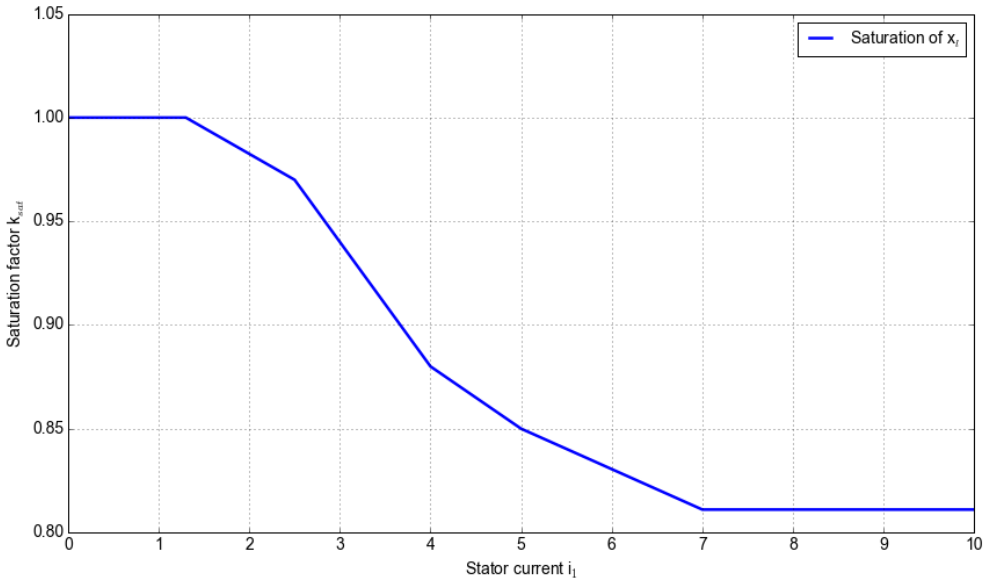

Figure 3-5: Saturation of stator leakage reactance

The behavior of the saturation factor as depicted in Figure 3-5 is only implemented in OpenModelica. The model in PowerFactory solely considers the lowest possible value of 0,811 resulting in a leakage reactance of 0,1574 p.u. and a subtransient reactance x_{dsat}'' of 0.3362 p.u..

The total moment of inertia J is composed of the respective contributions from the rotor, the turbine-runner as well as the water.

Table 3: Drive train data

given				calculated			
J_{Rotor}	$J_{Turbine}$	J_{Water}	J_{Total}	H_{Rotor}	$H_{Turbine}$	H_{Water}	H_{Total}
$*10^3$ kgm^2	$*10^3$ kgm^2	$*10^3$ kgm^2	$*10^3$ kgm^2	s	s	s	s
480	112,5	70	662,5	0,7295	0,171	0,1065	1,007

In OpenModelica elasticity and mechanical damping of the shaft are considered by connecting two gears representing generator inertia on the one hand and turbine-runner and water inertia on the other hand. The spring constant c is based on a reference torque value T_{ref}.

Table 4: Shaft data: spring and damping constant

calculated	
c	**d**
rad^{-1}	**-**
6,784	1

The grid strength has a large impact on the generator's response and its ability to stay in synchronism [16]. As depicted in Figure 3-6 for a fault with 0 p.u. remaining voltage, this impact is evident after fault clearance.

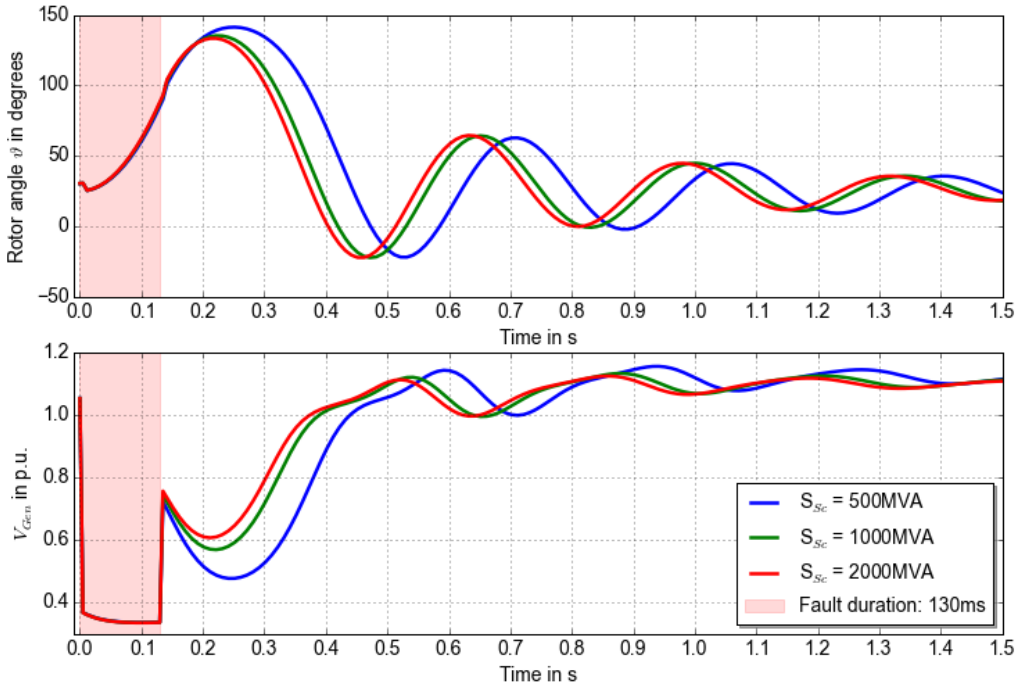

Figure 3-6: Impact of different grid short circuit capacities

The stronger the grid, the more rapidly the generator decelerates limiting the rotor angle excursions. To minimize the grid's influence a strong grid with a short circuit capacity of 2000 MVA is chosen.

Table 5: Grid data

Given			Calculated			
S_{Sc}	**U_n**	**c**	**$X_{Grid,HV}$**	**$X_{Grid,LV}$**	**$x_{Grid,HV}$**	**$x_{Grid,LV}$**
MVA	**kV**	**-**	**Ω**	**Ω**	p.u.	p.u.
2000	110	1	6,05	0,0405	1,98	0,01325

Table 6: Excitation system data

T_R	T_2	K_a	T_a	k	T	V_{amax}	V_{amin}	V_{imax}	V_{imin}
s	**s**	**p.u.**	**s**	**p.u.**	**s**	**p.u.**	**p.u.**	**p.u.**	**p.u.**
0,01	0,005	9,836	0,003	10,589	0,7	4	-4	5	-5

3.3 Fault simulation

The voltage sags at the grid connection point are simulated with both OpenModelica and PowerFactory. As explained in chapter 0, OpenModelica receives the voltage data from a table that specifies the remaining voltage and corresponding fault duration.

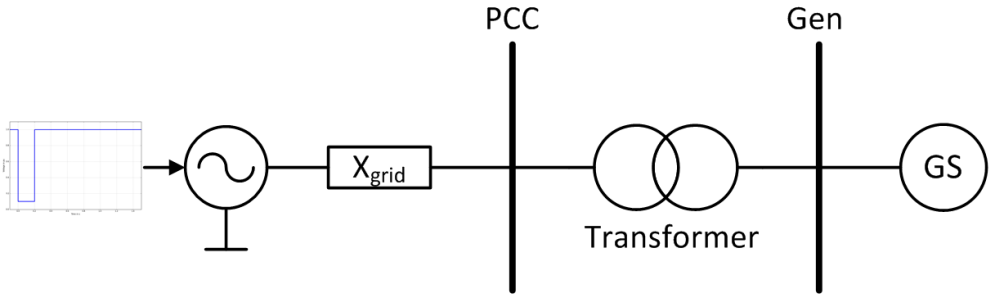

Figure 3-7: Fault simulation in OpenModelica

In PowerFactory, by contrast, the short circuit is activated by actuating a fault reactance connecting the PCC to ground.

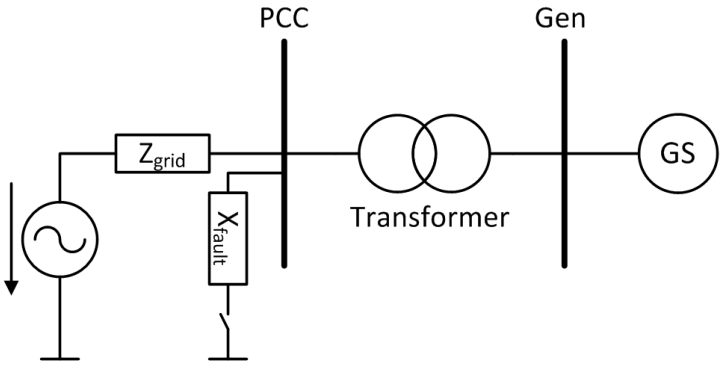

Figure 3-8: Fault simulation in PowerFactory

The desired remaining voltage during the fault is determined by the value of X_{fault} which can be derived by applying the rules of voltage division when the constant grid input voltage of 1 p.u. is distributed among Z_{grid} and X_{fault}:

$$V_{PCC} = \frac{X_{fault}}{Z_{grid} + X_{fault}} \cdot V_{grid} \rightarrow X_{fault} = \frac{V_{PCC}}{V_{grid} - V_{PCC}} \cdot Z_{grid} \tag{63}$$

Due to the grid reactance in the Modelica model, v_{PCC} never corresponds exactly to the rectangular profile given in the text file. The remaining voltage exhibits slight fluctuations as depicted in Figure 3-9. To ensure that the fault simulations in both environments are as similar as possible, the grid reactance X_{fault} in PowerFactory is dimensioned according to the average value of the remaining voltage $v_{PCC,average}$ in OpenModelica.

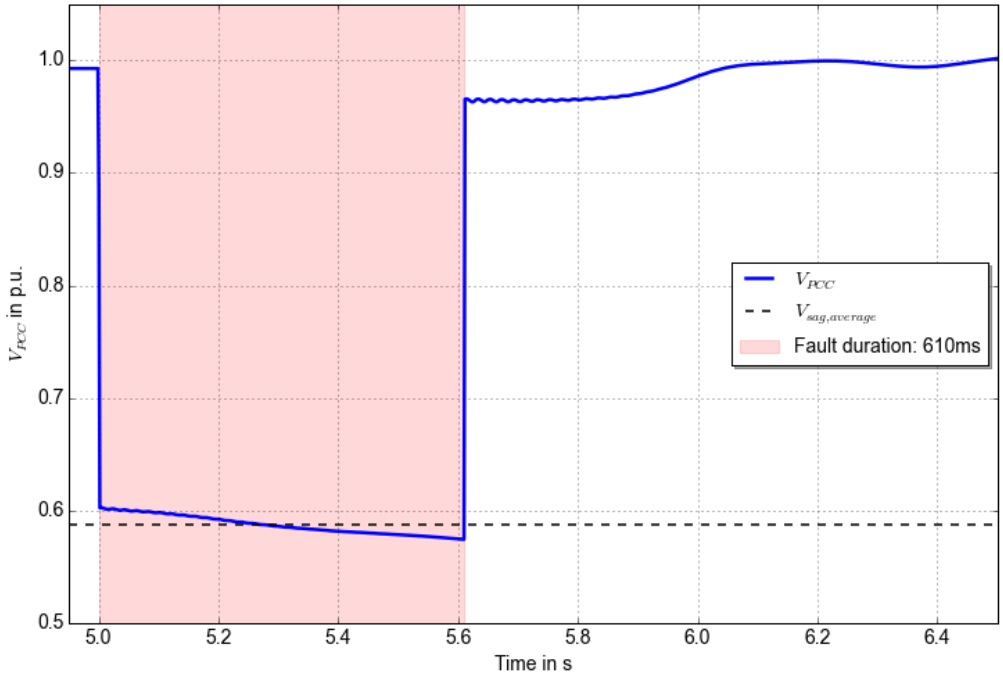

Figure 3-9: Actual remaining voltage at PCC in OpenModelica

The analysis of the LVRT capability leaves several degrees of freedom:

- Operating point of the generator (namely P and Q)
- Remaining voltage during the fault
- Fault duration

In Modelica the generated active power P_{Gen} is determined by the hydraulic turbine characteristic. Hydraulic curves are provided for three different operating points: 91%, 75% and 55% loading corresponding to 21,7 MW, 17,8 MW and 13,1 MW, respectively. The reactive power Q_{Gen} can be varied within the limits of the generator output diagram. 21,7 MW and a leading power factor of 0,9 (i.e. under-excited) constitutes the most critical operating point with regard to rotor angle excursions. Figure 3-10 shows the impact of excitation and loading on the steady state rotor angle. It is evident that higher loading and lower excitation increases ϑ_0 reducing the synchronizing torque available and pushing it closer to its stability limit.

The voltage sag is varied between 0% and 90% remaining voltage while the fault duration is stepwise increased from 50 ms until the critical clearing time t_{cc} (i.e. the stability boundary) is reached. The critical clearing time is a measure of power system robustness to withstand large disturbances which includes relay, communication and breaker operation times.

The determination of t_{cc} is visualized in Figure 3-11. Obviously the system is transiently unstable for a sag with 0 p.u. remaining voltage and a clearing time exceeding 110ms. For any clearing time t_c less than t_{cc} the system is *transiently stable* or *first-swing stable*. Consequently, the transient stability of the system can be determined for any given clearing time t_c without numerical simulations if the critical clearing time is known. This allows the definition of a stability measure [5]:

$$M_t = \frac{t_{cc} - t_c}{t_{cc}} \cdot 100\% \tag{64}$$

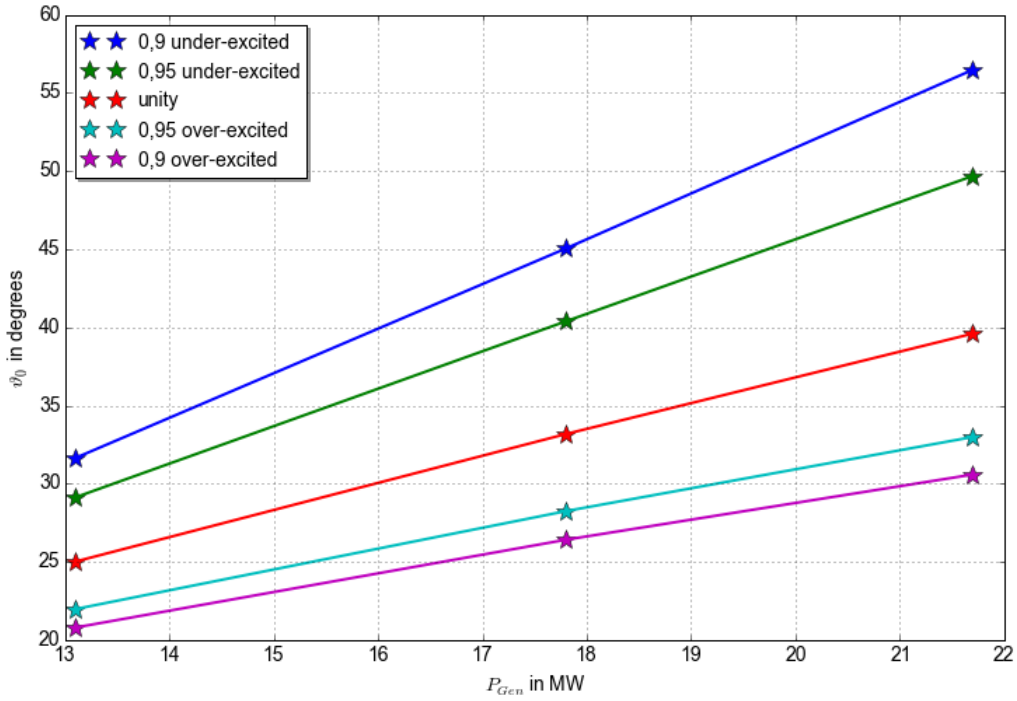

Figure 3-10: Rotor angle as a function of excitation and loading

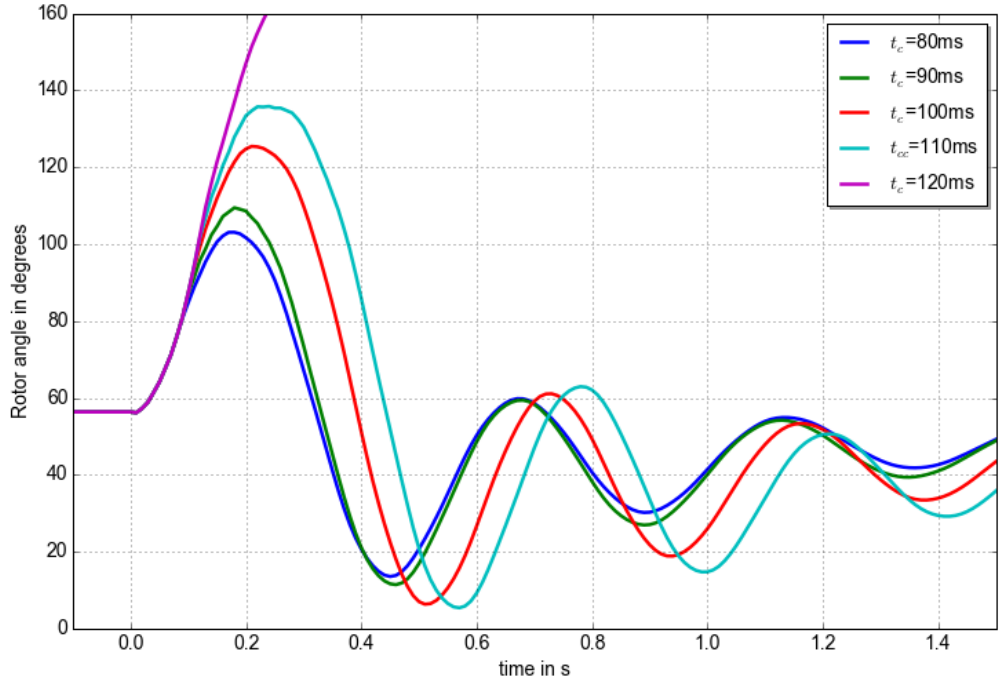

Figure 3-11: Variation of rotor angle with fault clearing time

Table 7 contains the stability measures for the cases illustrated in Figure 3-11. Increasing M_t enhances transient stability.

Table 7: Stability measure for different clearing times

t_c	M_t
ms	**%**
80	27,3
90	18,2
100	10
110	0

The iterative process to determine the stability boundary for a given operating point is visualized in Figure 3-12. The remaining voltage is increased from 0 p.u. to 1 p.u. in steps of 0.1 p.u. while the fault clearing time is increased in steps of 10 ms.

At first, a simulation is run in OpenModelica to determine the parameters required for initialization in PowerFactory, namely the excitation voltage V_{ex} and the steady state voltage at the grid connection point V_{PCC}. As soon as these parameters are known, a load flow can be performed in PowerFactory serving as a starting point for further simulations.

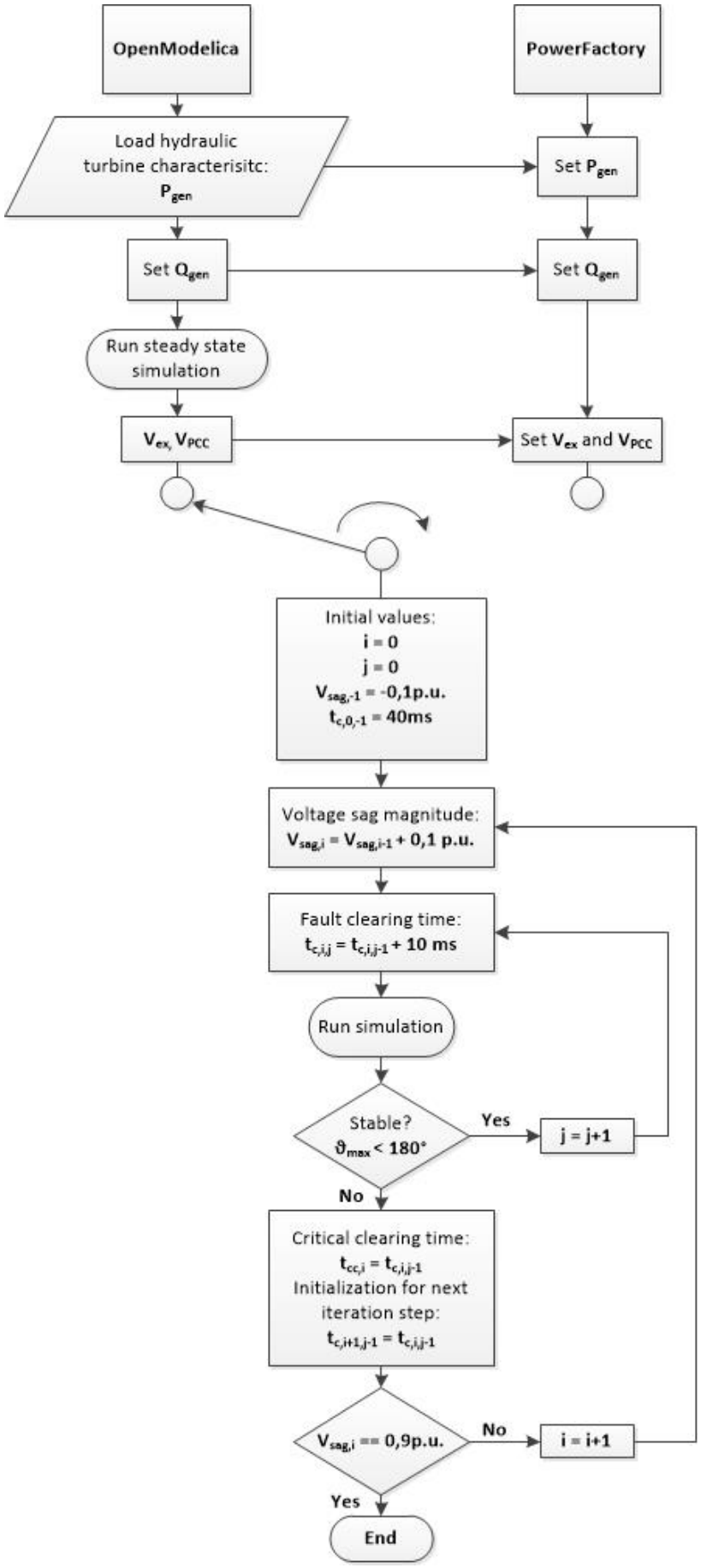

Figure 3-12: Iteration process to determine critical clearing time

3.4 Results and discussion

3.4.1 Comparison of OpenModelica and PowerFactory

Initially, the simulation results of OpenModelica and PowerFactory are compared for a fault with 0 p.u. remaining voltage and a duration of 100 ms. The operating point is chosen at 21,7 MW and rated power factor (i.e. over-excitation).

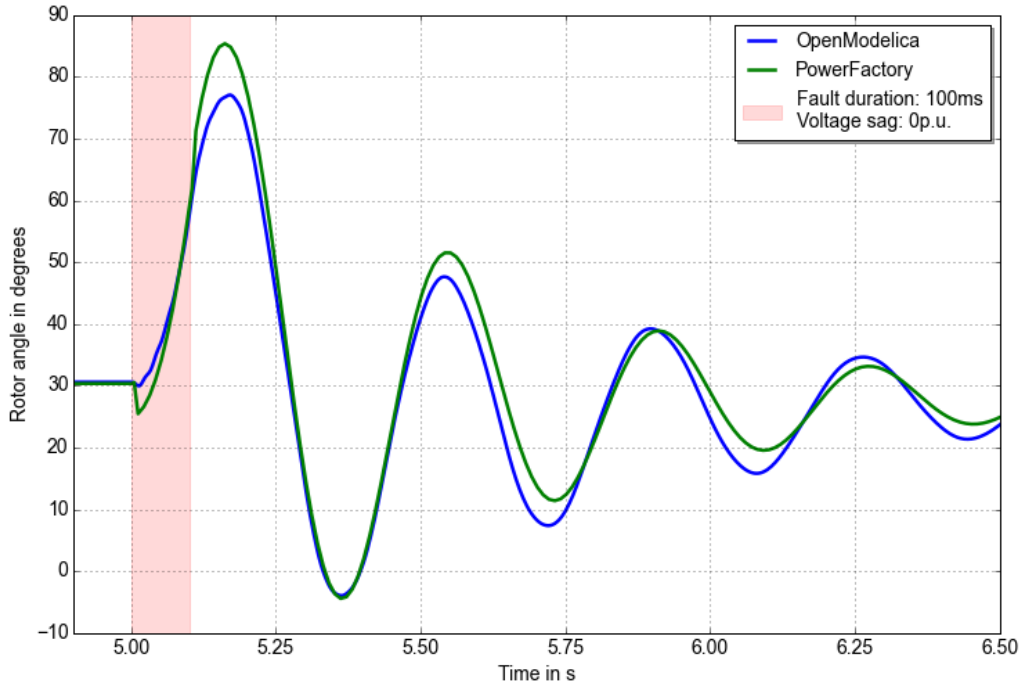

Figure 3-13: Comparison of rotor angles (OpenModelica vs. PowerFactory)

It can be observed that damping is increased with the Modelica model. This is for one part due to the implemented saturation model of the stator leakage reactance which influences the transient electrical behavior of the machine. Saturation is especially significant at high current levels, e.g. during short-circuits (see Figure 3-5) where reduction in x_l of up to 25% compared to unsaturated values are possible.

Increased damping can further be attributed to the hydraulic system. Figure 3-14 shows the difference in rotor angle oscillations between the detailed model (blue) and a constant torque model in OpenModelica neglecting the hydraulic system (green).

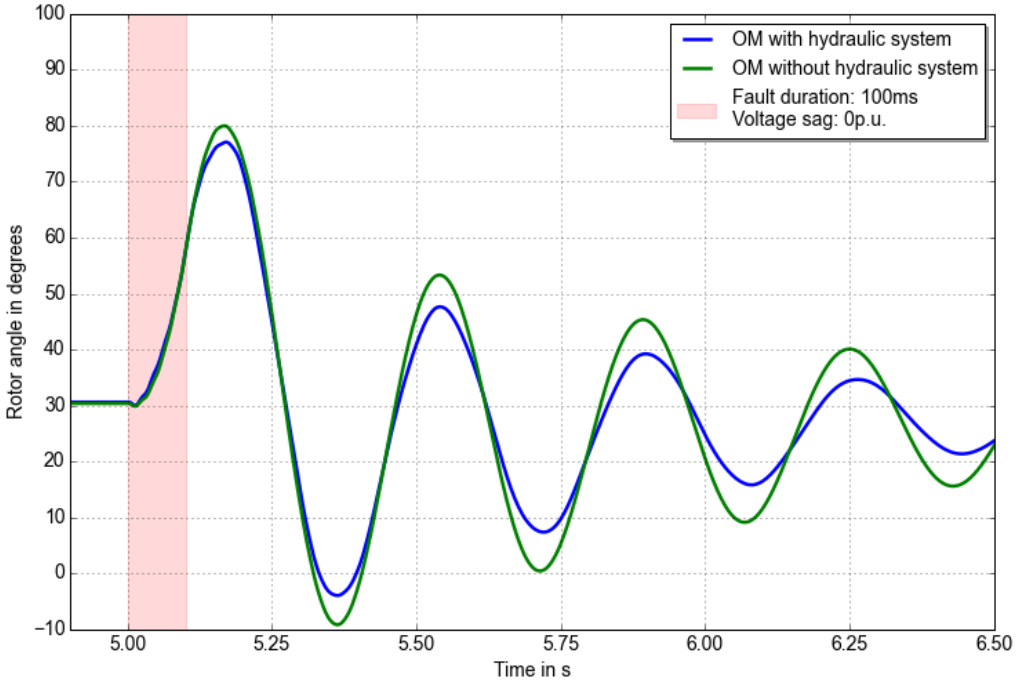

Figure 3-14: Influence of the hydraulic system on damping

Thus, it can be concluded that the deviation of the results obtained in PowerFactory with respect to the outcomes in OpenModelica can as well be traced back to the pipe and turbine models of the hydraulic system.

The consequence of neglecting the stator flux transients in RMS simulations is evident in Figure 3-15 and Figure 3-16 where high-frequency oscillations in the generator terminal voltage as well as the generator active and reactive power cannot be represented entirely. Only the fundamental components of voltages and currents are taken into account.

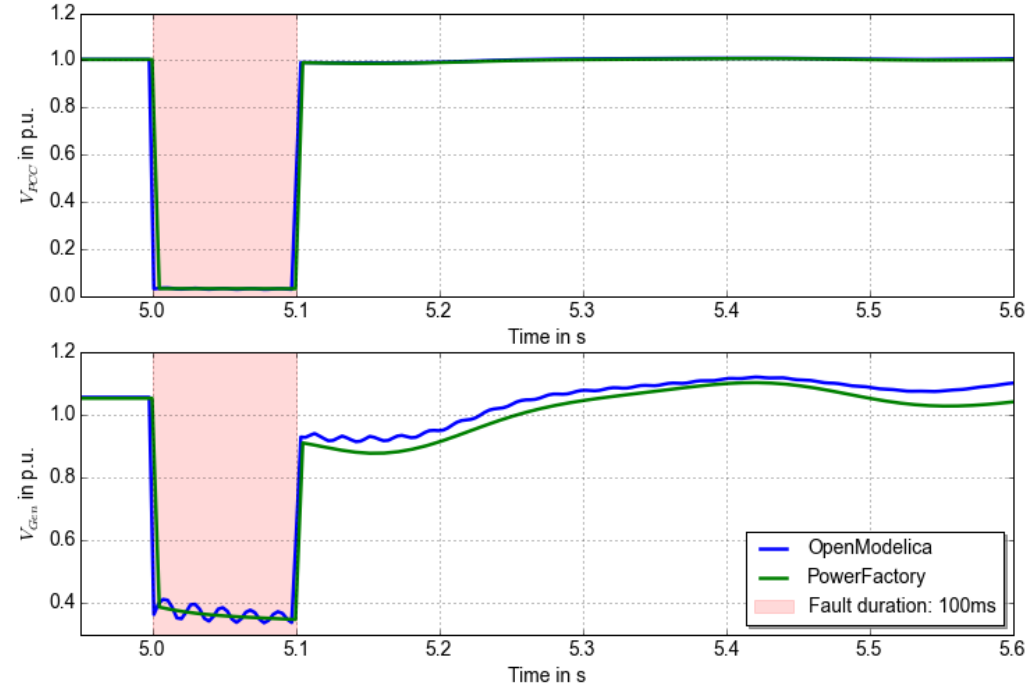

Figure 3-15: Comparison of voltages at PCC and Gen bus bar (OpenModelica vs. PowerFactory)

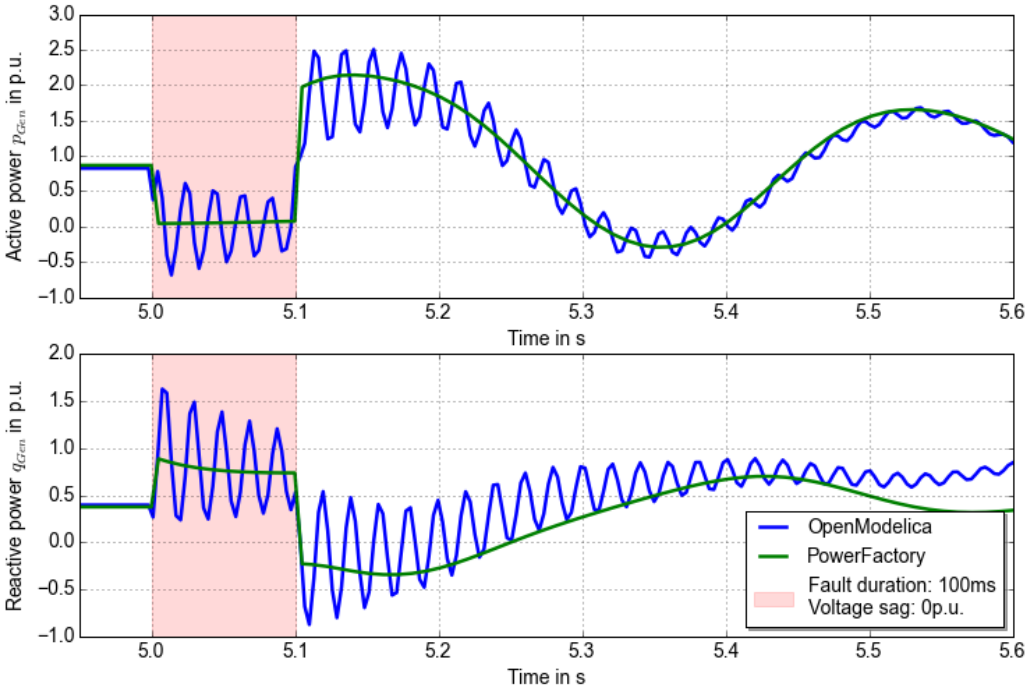

Figure 3-16: Active and reactive power (OpenModelica vs. PowerFactory)

Even though the same exciter and AVR are used, the results in Figure 3-17 reveal that they still do not exhibit the same response in the aftermath of a fault. However, this deviation can also be attributed to the saturation model which is not fully implemented in PowerFactory. The blue curve only demonstrates the excitation voltage when a generator model is used that is based on already saturated values of the stator leakage reactance. The actual model itself which continuously adjusts the value of x_l depending on the stator current is not included.

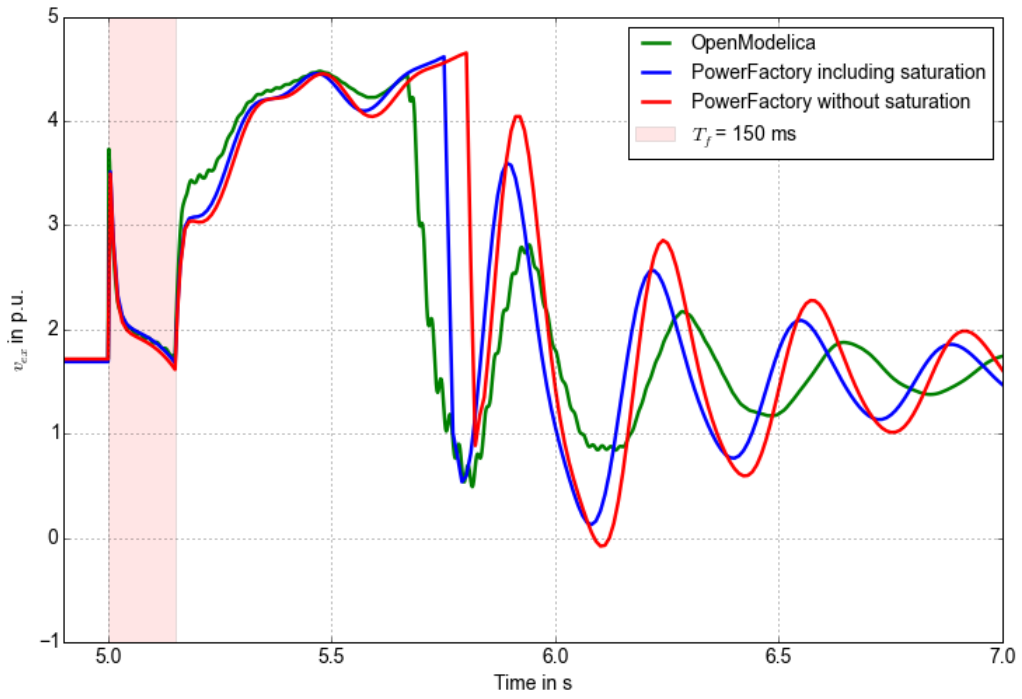

Figure 3-17: Comparison of excitation voltages

3.4.2 Grid code compatibility

In the following the solutions for the worst case, namely 91% loading and under-excited power factor (Q = -10,5 Mvar), are presented whereas those referred to other operating points are included in the appendix.

ϑ_{cc} is the critical clearing angle which is the corresponding rotor angle to t_{cc}. It can be analytically determined by applying the Equal Area Criterion. The relationship between t_{cc} and ϑ_{cc} is given by

$$t_{cc} = \sqrt{\frac{2T}{P_m - P_e^f} \cdot (\vartheta_{cc} - \vartheta_0)} \tag{65}$$

where T, P_m, P_e^f and ϑ_0 represent the torque, mechanical power, electrical power during the fault and pre-fault rotor angle, respectively. Equation (65) is only valid if P_e^f is a constant. Otherwise t_{cc} has to be determined numerically.

Table 8: Critical clearing time and angle for 21,7 MW and -10,5 Mvar (worst case)

	OM			PF		
V_{PCC}	t_{cc}	ϑ_{cc}	M_t	t_{cc}	ϑ_{cc}	M_t
%	ms	deg	%	ms	deg	%
0	110	136	-26,7	90	124	-40
10	120	137	-60	100	123	-66,7
20	140	145	-68,9	120	130	-73,3
30	160	139	-73,3	150	144	-75
40	200	147	-73,3	190	143	-74,7
50	270	152	-70	240	138	-73,3
60	610	151	-41,9	460	145	-56,2

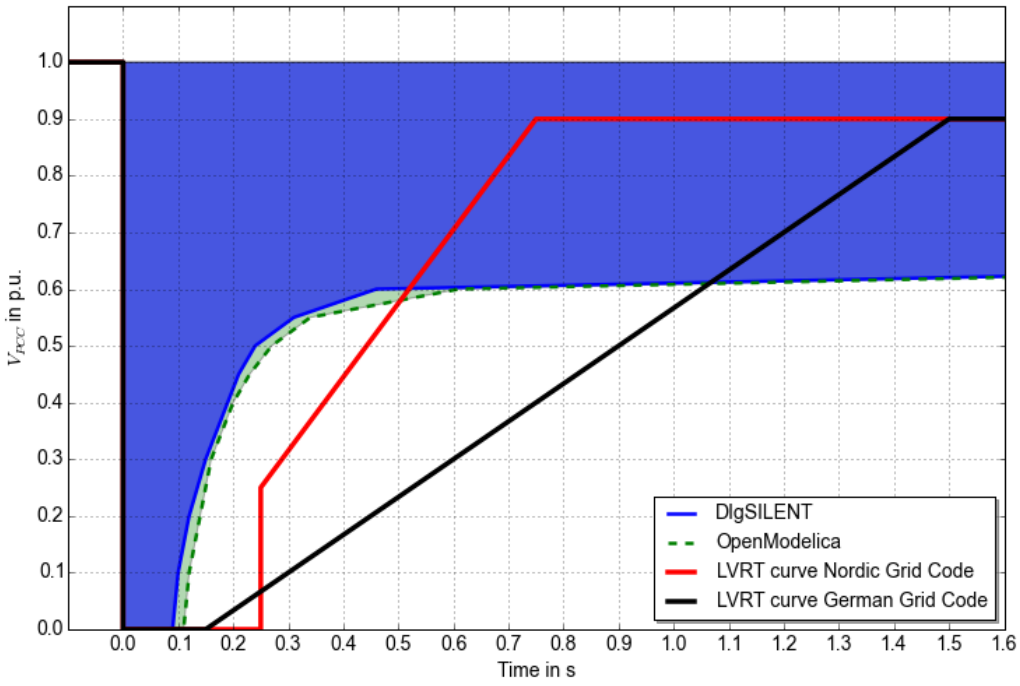

Figure 3-18: Stability region OpenModelica vs. PowerFactory (critical operating point)

Figure 3-18 shows the stability region of the machine as a function of the critical clearing time compared to the German and Nordic LVRT curves. The dashed line represents the additional stability provided by the Modelica model.

Apparently, increased damping due to saturation and hydraulic characteristics does not yield any considerable benefits regarding LVRT capability. The machine does not fulfill the grid code requirements neither in under-excited nor in over-excited operation (Figure 3-19). Although decreasing the machine loading enhances transient stability, the generator still does not comply with any of the grid codes, not even for less severe operation points (see appendix).

Table 9: Critical clearing time and angle for 21,7 MW and 10,5 Mvar

	OM			PF		
V_{PCC}	t_{cc}	ϑ_{cc}	M_t	t_{cc}	ϑ_{cc}	M_t
%	ms	deg	%	ms	deg	%
0	160	149	6,3	140	135	-6,7
10	180	145	-40	160	141	-46,7
20	210	143	-53,3	190	145	-57,8
30	270	153	-55	240	147	-60
40	430	152	-42,7	400	158	-46,7

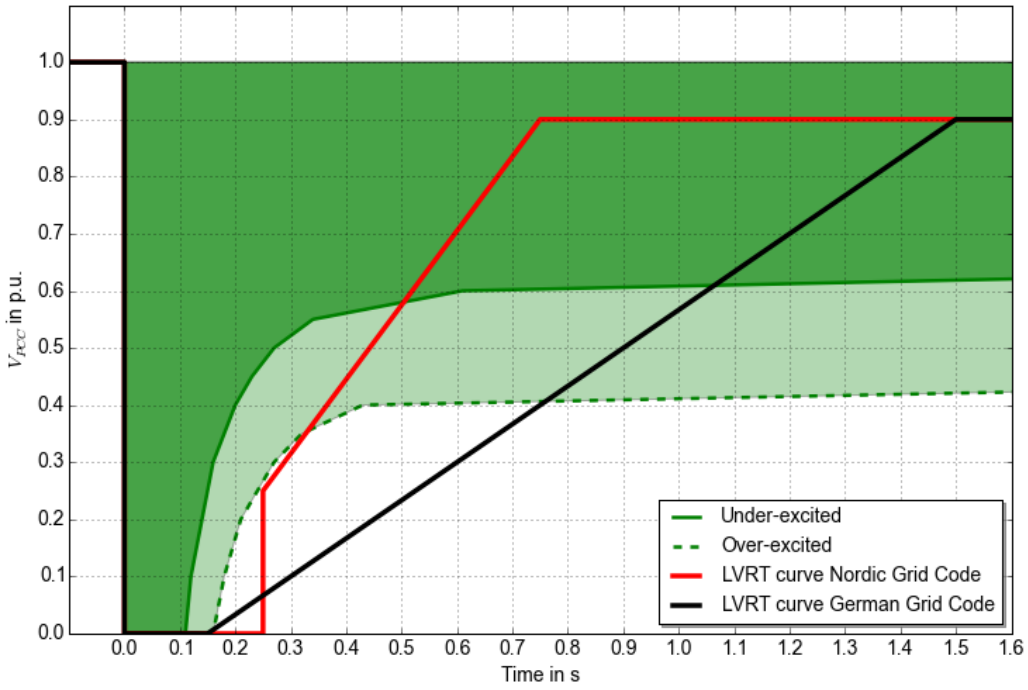

Figure 3-19: Stability region under-excited vs. over-excited operation (P = 21,7 MW)

Thus, it can be concluded that generator transient stability depends on the loading of the machine, the fault clearing time, the internal voltage magnitude that is determined by the field excitation and the voltage magnitude at the grid connection point. Additionally, a lower generator reactance reduces the initial rotor angle while higher inertia damps the rate of change in angle contributing to generator robustness [3]. Solutions to avoid tripping of the machine are discussed in the next chapter. Further simulations are only carried out in OM given the similarity of the results.

4 Improvement of system stability using braking resistors

There are several approaches to enhance transient stability by the use of supplementary controls which include among others series and shunt capacitor compensation, high-speed excitation systems with AVRs and Power System Stabilizers as well as power electronics based controllable devices (FACTS). Additionally, these actions can improve damping of electromechanical oscillations.

Another more simple but effective method is the use of braking resistors (BRs) where a shunt or series resistor close to the generator is activated for a short time following a fault diminishing the rotor acceleration. Conventional braking resistors are inserted in parallel with the generating unit. Yet, their effectiveness is limited during severe voltage sags due to the quadratic relationship between dissipated power and voltage. A series BR is more favorable considering its *current-squared* relationship to power dissipation [23].

In this thesis a model using one single three phase series braking resistor (SBR) that dissipates active power during a fault is investigated. Figure 4-1 illustrates the basic approach to the following task.

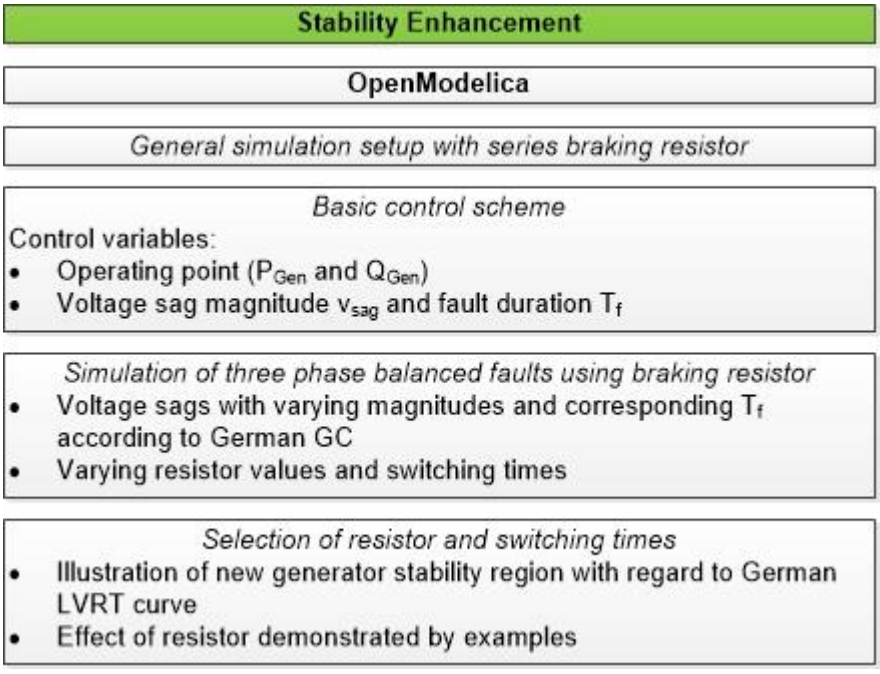

Figure 4-1: Approach to improve system stability

4.1 Applications of braking resistors

The concept of BRs is not an entirely novel technology. It has been widely implemented in decentralized power plants, among others in the wind industry. Nowadays, even wind farms are required to remain connected and actively contribute to system stability during fault events.

Pitch control and dynamic reactive power compensation are the most commonly deployed LVRT strategies for wind turbines. However, these state-of-the-art techniques are limited, particularly blade pitching where the mechanical loads imposed on a wind turbine during power restoration are onerous. A series resistor in the generation circuit converting electrical energy into heat eliminates the need for pitch control by supporting the voltage at the generator terminals and thereby reducing the destabilizing decline of electrical torque and power during the fault. Furthermore, SBRs provide faster power control than blade pitch regulation [17] [23].

Another application of dynamic BRs is the support of transient stability and the enhancement of the overall dynamic performance of a power system rather than individual power plants. For this purpose the stabilizing component is activated after fault clearance and voltage recovery, not during a fault. They are implemented in many power systems around the world. The Bonneville Power Administration (BPA), for example, TSO in the Pacific Northwest (USA), installed a BR at the Chief Joseph Substation in the early 1970's. This measure increased the transmission capacity of the intertie-lines between the NW and California (see Figure 4-2). The resistor, capable of dissipating 1400 MW, is switched onto a 230 kV substation bus [24].

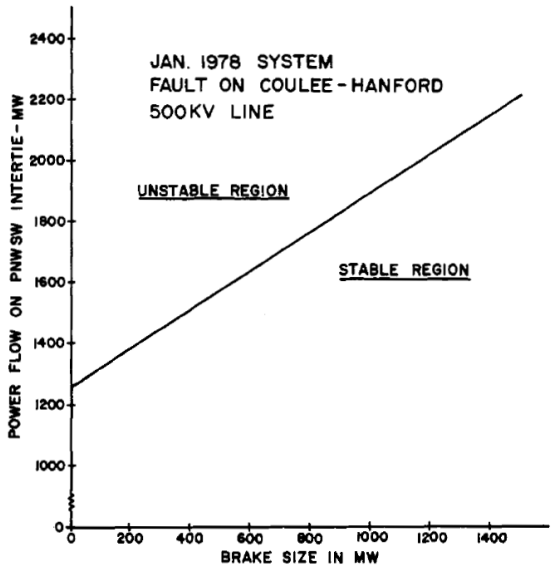

Figure 4-2: Influence of BR size on PNW-California intertie capacity [24]

The control system comprises two power rate relays located at Chief Joseph and John Day Substation which measure the acceleration power during grid disturbances. If measured power exceeds a preset value and generator bus voltage drops, a *close signal* is sent to the brake controller inserting the brake for a short duration during the first swing of a transient disturbance [25].

Controllable active power sink devices connected to the terminals of a generator are another possible solution to fulfill LVRT requirements. A switched series resistor and a converter controlled shunt component are triggered by the remaining voltage during the fault and the pre-fault voltage phasor angle, respectively. Low as well as high series resistor values can be used to overcome shortcomings regarding LVRT [18].

4.2 Simulation setup and basic control scheme

Lower voltage levels at the connection point entail that less active power can be injected into the grid. The mechanical input power to the generator remains constant though, perturbing the balance between generated and dissipated power which causes the rotor to accelerate.

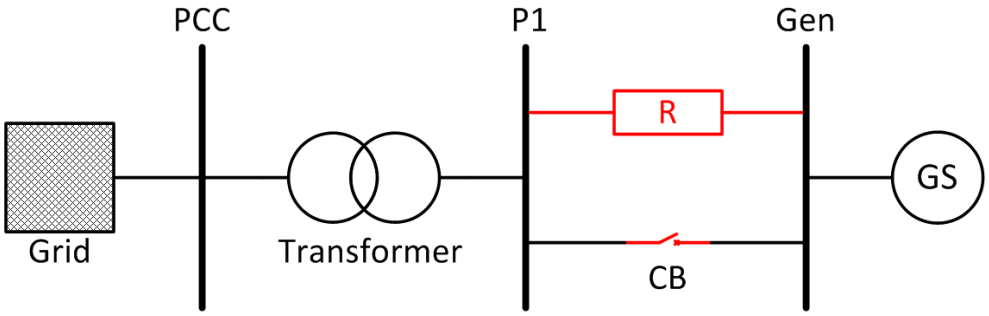

Figure 4-3: System under test including breaking resistor

The system in OpenModelica is extended with an ohmic braking resistor between the generator terminals and the transformer to increase both the dissipation of active power and the voltage at the generator terminals during a fault. The component could be placed on the transformer's primary side as well but would be exposed to higher voltages and thus require higher insulation efforts. Given that the problem of insufficient power dissipation arises only during fault events, the resistor is inserted upon fault detection and bypassed otherwise.

A BR in the generator circuit increases I^2R-losses and exhibits a self-stabilizing behavior. The short circuit current depends on the voltage sag magnitude. The lower the remaining voltage, the higher the fault current and power imbalance will be leading to increased dissipation in the resistor which in turn compensates for the power imbalance [12].

To avoid unnecessary losses in steady state operation the resistor is only activated during a fault and has to be inserted as quickly as possible to maximize the braking effect. Thyristor controlled switches have the advantage of very short switching times (~25 ms) but cannot be used due to the high short circuit currents. Instead, a circuit breaker is installed activating the resistor within 80 ms after fault occurrence. The risk of high activation times is that the acceleration of the rotor might be too advanced to be slowed down efficiently.

A fault detection control logic triggers the circuit breaker depending on measured remaining voltage during a fault and pre-fault operating point of the generator. A realistic resistor activation time of 80 ms is assumed including approximately one cycle of fault detection (20 ms) and 60 ms of insertion time.

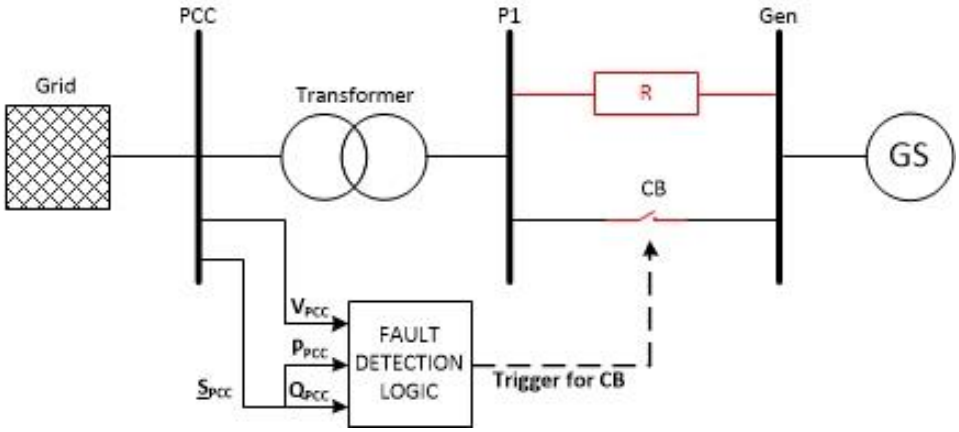

Figure 4-4: Basic fault detection logic concept

The input signals for the fault detection logic are measured at the PCC where active and reactive power are determined by P_{Gen} and Q_{Gen} and adjusted according to the transformer reactive power consumption as well as active power losses. Table 10 shows the reactive power conditions tested on the machine when producing 21,7 MW and referred to both generator as well as grid connection bus bar.

Table 10: Relationship between reactive power conditions at Gen and PCC bus bar

P = 21,7 MW					
Operating point	**Q_{Gen}**	**$\cos(\varphi_{Gen})$**	**Q_{Gen}/P_{max}**	**Q_{PCC}**	**$\cos(\varphi_{PCC})$**
No.	**Mvar**	**-**	**-**	**Mvar**	**-**
1	-10,5	0,9 under-excited	-0,44	-14,46	0,83
2	-7,13	0,95 under-excited	-0,29	-10,51	0,9
3	0	1	0	-2,77	0,99
4	7,13	0,95 over-excited	0,29	4,32	0,98
5	10,5	0,9 over-excited	0,44	7,49	0,95

Grid codes also specify requirements for reactive power supply from generating units. For operation at an active power output below nominal conditions ($P < P_n$), the generator must be capable to operate in every possible working point according to its own output diagram (i.e. PQ-diagram) respecting armature current, field current and end region heating limits [21]. The machine under test is usually operated with a power factor of 0,9 or higher in under- as well as over-excited operation and is not expected to exceed this boundary. Present reactive power supply requirements are usually formulated by a U-Q/P_{max} profile.

Figure 4-5 shows the faults and pre-fault reactive power conditions for 21,7 MW which are not GC compatible and require additional stabilizing measures. The voltage sag at the connection point during the fault is plotted on the y-axis with a fault duration T_f according to the German GC (Table 11). Red dots indicate that the generator loses synchronism for the considered operating point when subjected to the respective voltage depression at its terminals, thereby raising the need for additional measures to achieve GC compatibility.

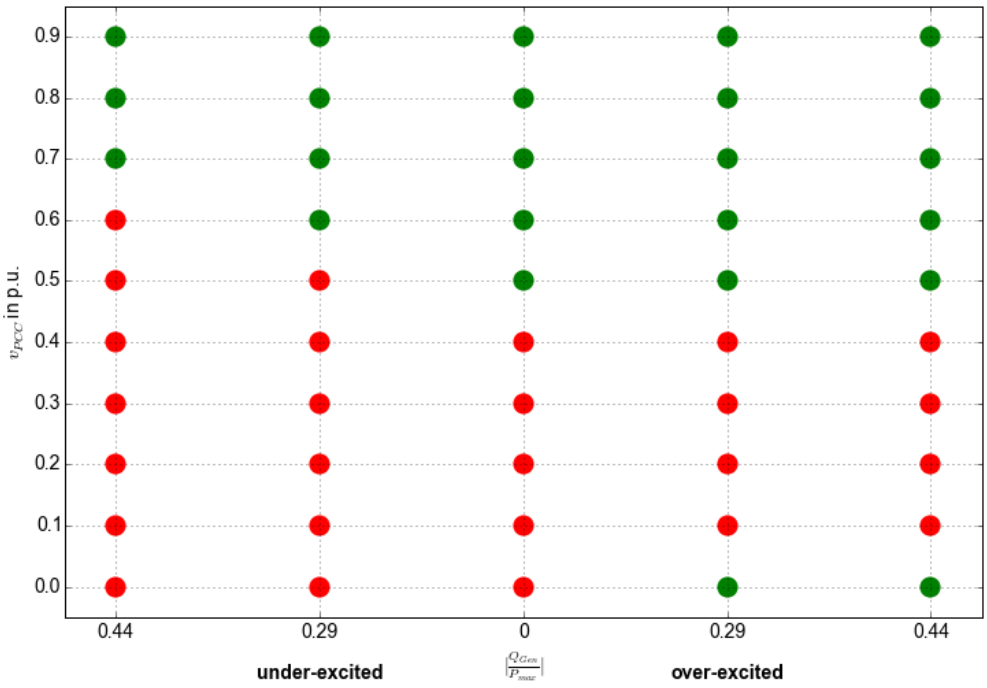

Figure 4-5: Faults requiring insertion of BR (P = 21,7 MW)

Table 11: Simulated faults according to German GC

v_{sag}	T_f	v_{sag}	T_f
p.u.	**ms**	**p.u.**	**ms**
0	150	**0,5**	900
0,1	300	**0,6**	1050
0,2	450	**0,7**	1200
0,3	600	**0,8**	1350
0,4	750	**0,9**	1500

The fault detection control logic triggers the CB corresponding to the results in Figure 4-5. It can be observed that the resistor is never activated for faults with remaining voltages above 70% of the nominal value since those cases are stable (i.e. GC compatible) without any additional actions. The equivalent illustrations for 17,8 MW and 13,1 MW are included in the appendix.

4.3 Selection of resistor and switching time

Compared to the fault simulations for determining the machine's LVRT capability in chapter 3, including a resistor in the analysis leaves two additional degrees of freedom:

- Resistor value
- Resistor on-time (i.e. CB closing time)

The optimal value of the BR to successfully restore power balance depends on the operating point of the generator as well as the voltage sag magnitude during a fault. Hence, changing circumstances require different resistor values to achieve the optimum. In practical applications however one resistor should be able to cover all possible incidents. Its value is determined in an iterative process [12].

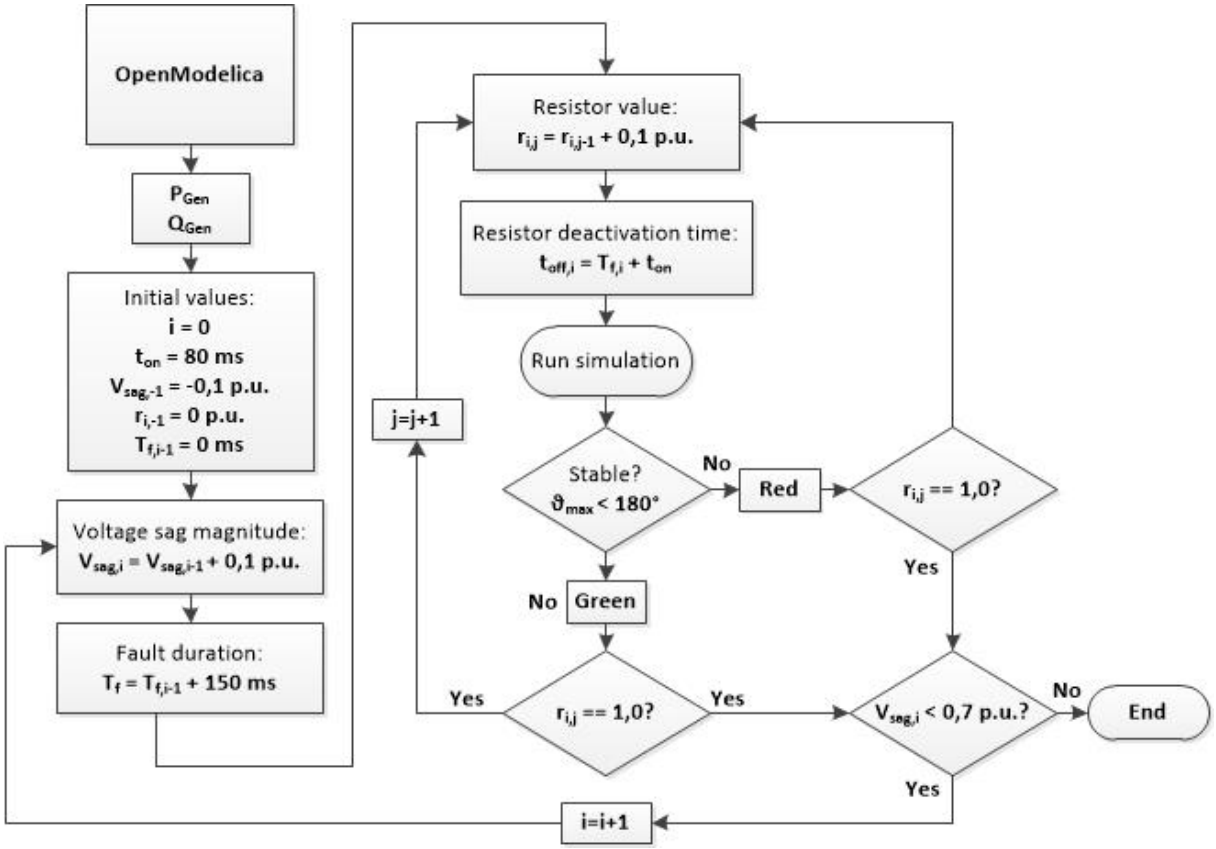

Figure 4-6: Iterative process to determine resistor value range for P = 21,7 MW and Q = -10,5 MVar

Again, the operating point of the machine is set to 21,7 MW and a power factor of 0,9 under-excited to achieve the worst case scenario for evaluating appropriate values of the two above mentioned variables. As depicted in Figure 4-5, this operating point is not GC compatible for any fault with a remaining voltage less than 70% of the nominal value. For a pre-defined voltage sag with corresponding fault duration the resistance is stepwise increased from zero until all stability criteria are fulfilled. They are usually met not only by one single resistor value but rather by a whole range of values. As soon as the lower limit of the scope is known, the value is further increased until the upper boundary of the stability region is found. Then, the voltage sag magnitude is increased while the fault duration as well as the resistor deactivation time are adapted accordingly. The process is repeated to evaluate the new resistor value range. Overlapping the resulting value ranges yields a resistor value for the worst case scenario that can cover different faults.

In a first approach, the resistor is activated 80 ms upon fault occurrence (t_{on}) and remains in the circuit for the duration of the fault. The CB is actuated at fault clearance, entirely deactivating the resistor 80 ms later. The deactivation time including the time delay of 80 ms is termed t_{off} in the following while the total duration for which the BR remains in the circuit is

named T_{act}. The minimum duration and CB closing time to achieve GC compatibility contain the additional subscript *min*.

$$T_{act} = t_{off} - t_{on} \tag{66}$$

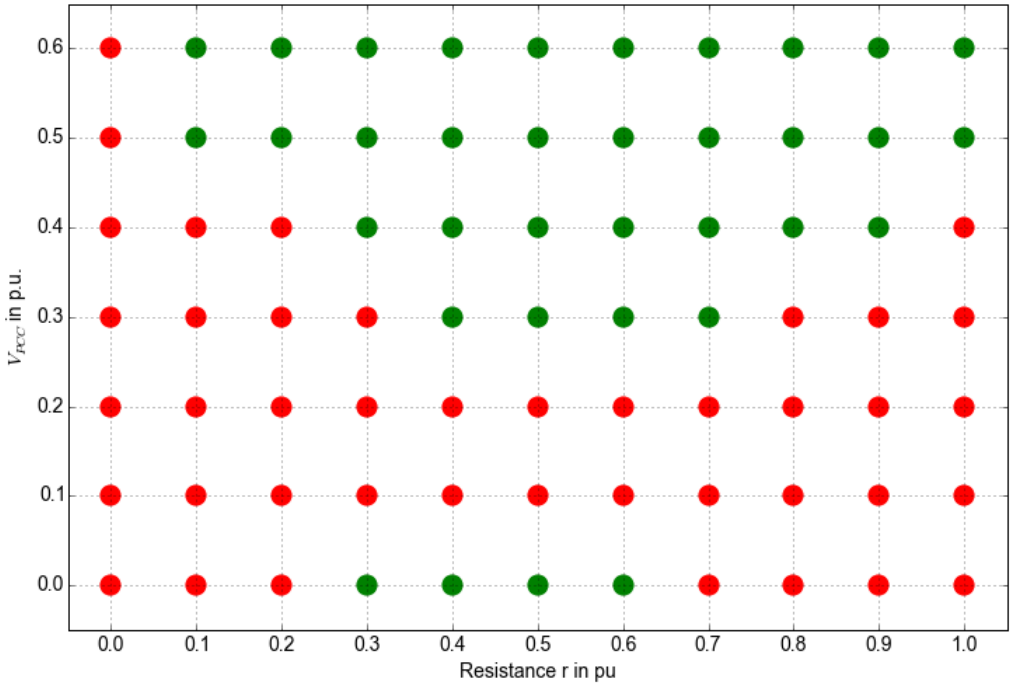

Figure 4-7: Stabilizing effect of BR with varying values for worst case scenario

It can be observed that a resistance in the range of 0,4 p.u. and 0,6 p.u. is able to cover most of the faults (Figure 4-7). However, voltage sags to 10% and 20% U_n are most critical due to the combination of severe voltage depth and long fault duration (300ms and 450ms, respectively). For these faults and an activation time of 80 ms no resistor value regardless of its on-time is sufficient enough for the machine to remain in step.

4.3.1 Critical fault events

A more detailed analysis of the critical fault events with 10% and 20% remaining voltages is carried out. Hereby, the fault duration, the resistor value as well as the resistor on-time are varied. The maximum fault duration the generator can be exposed to without losing synchronism is investigated depending on the resistor value and the minimum on-time. Table 12 contains the critical clearing times depending on the resistor value while Figure 4-8 illustrates it graphically.

Table 12: Critical clearing time and minimum on-time for v_{PCC} = 0,2 p.u.

R	t_{cc}	$t_{off,min}$
p.u.	ms	ms
0	140	-
0,1	170	260
0,2	210	330
0,3	240	340
0,4	270	360
0,5	280	360
0,6	280	360
0,7	260	340
0,8	240	340
0,9	220	350
1	200	370

The German GC specifies for a fault with 20% remaining voltage a duration of 450 ms. However, the maximum clearing time that can be achieved with resistances of 0,5 p.u. and 0,6 p.u. is limited to 280 ms (highlighted in yellow). Since neither changing the resistance nor the on-time of the resistor helps to achieve GC compatibility, the activation time t_{on} is varied. It can be seen in Figure 4-8 that a reduced activation time increases the fault duration that can be overcome.

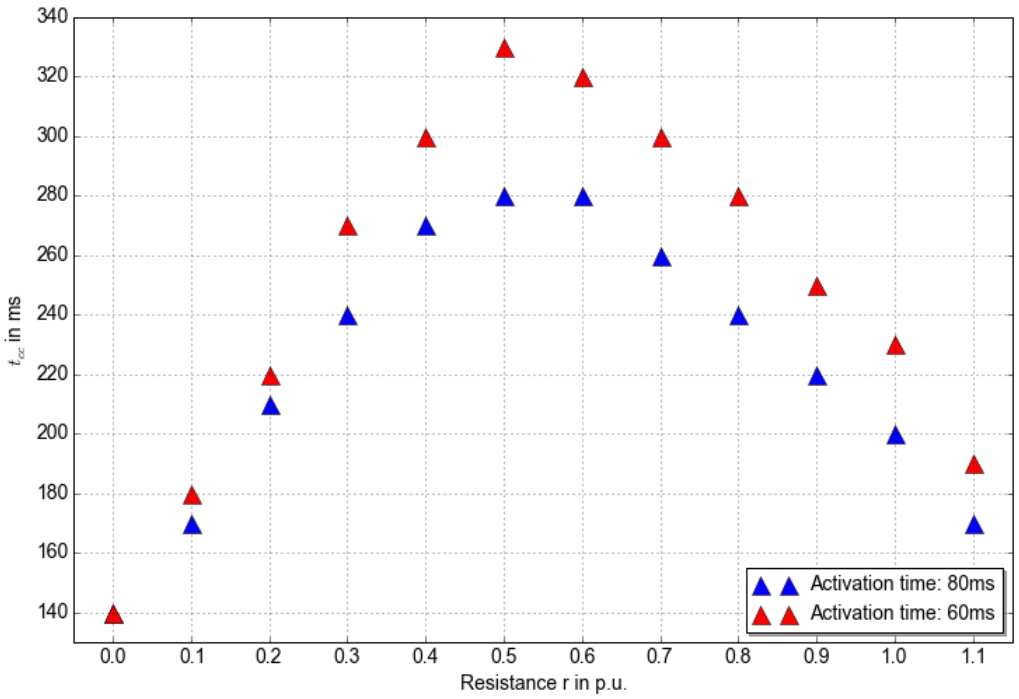

Figure 4-8: Critical clearing time with varying BRs for a fault with 0,2 p.u. remaining voltage

4.3.2 Non-critical fault events

In the next step, the other single fault events are analyzed in more detail. The minimum deactivation time $t_{off,min}$ is investigated for various resistor values. Hence, the iterative process is extended by an additional loop increasing t_{off} by 10ms after each iteration until the stability criteria are fulfilled.

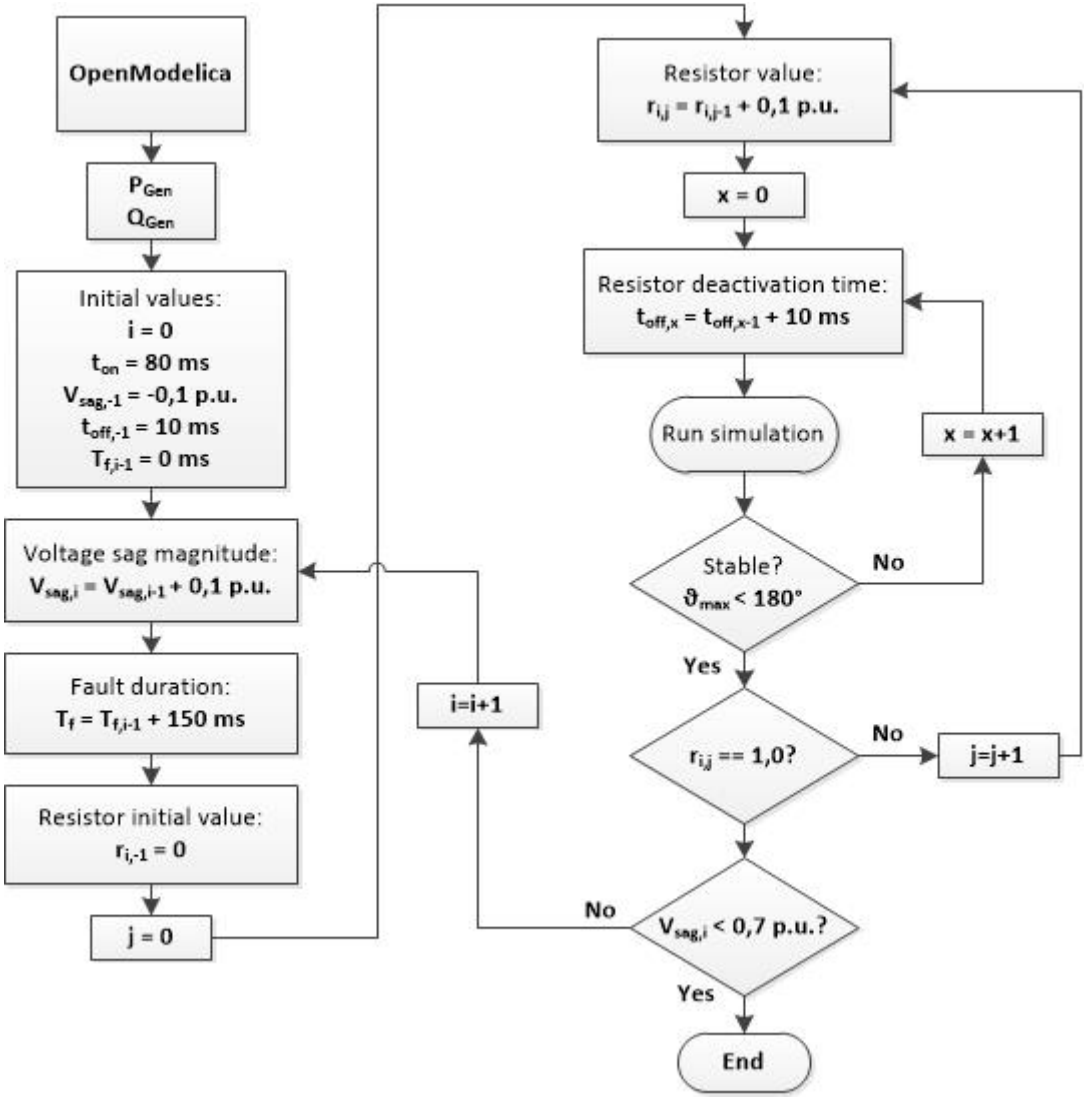

Figure 4-9: Iteration process to determine resistor value and respective on-time

A voltage depression with 50% remaining voltage and a duration of 900 ms can be tolerated with resistors in the range of 0,1 p.u. and 1,0 p.u. as depicted in Figure 4-10. It can be observed that for 0,4 p.u. and 0,5 p.u. the resistor can be switched off a lot earlier than with other resistances. Considering this and the fact that the longest fault durations for critical faults which can be tolerated are achieved with a resistor of 0,5 p.u. (see Figure 4-8), the corresponding absolute value of 1,53 Ω is chosen for the considered machine setup.

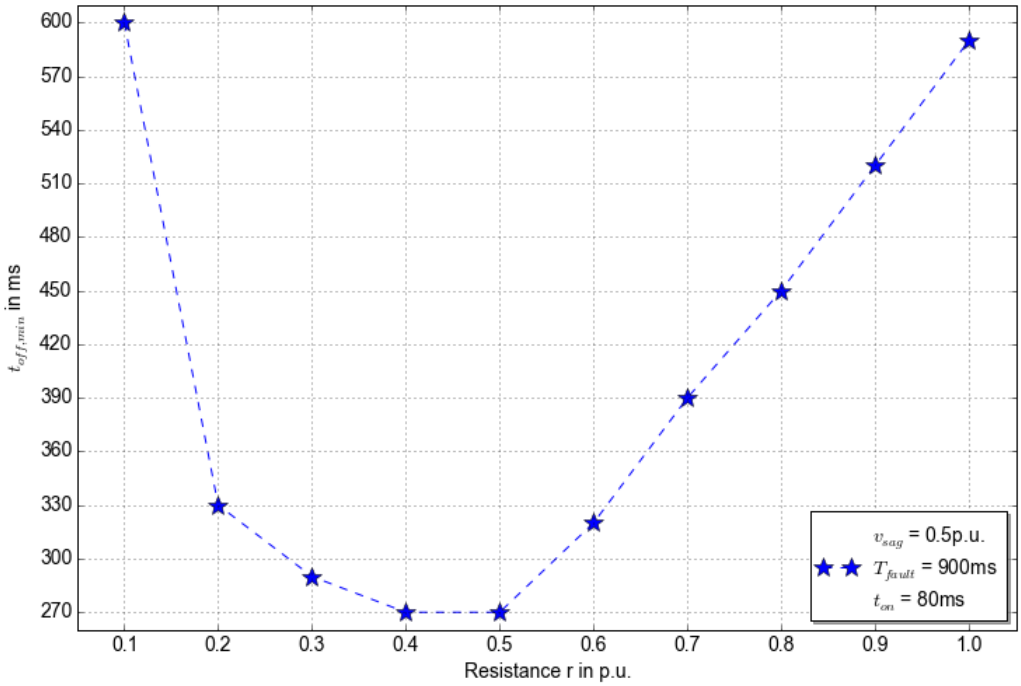

Figure 4-10: $t_{off,min}$ as a function of resistance (worst case operating point)

Dissipated power can also be expressed in terms of energy. Figure 4-11 shows the absorbed energy as a function of the resistor value. Hereby, the operating point is chosen with approximately 50% loading and over-excited power factor to achieve GC compatibility over a wide range of resistor values. The resistor on-time remains equal for all cases (i.e. 120 ms). Energy is expressed as a product of active power in p.u. and time in s based on a time reference value of 1 s, namely [(Ws)/(VAs)] [18].

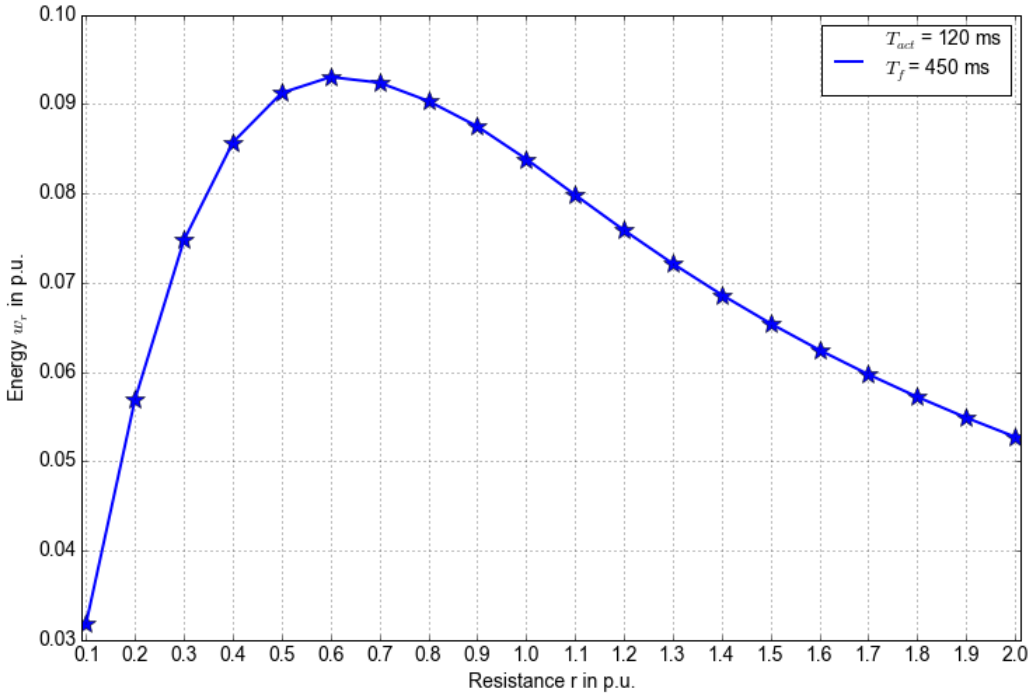

Figure 4-11: Absorbed energy as a function of resistor value with equal insertion duration (v_{PCC} = 0,2 p.u., P = 13,1 MW, pf = 0,9 over-excited)

However, adjusting the on-time to the respective resistor values by reducing the CB closing time to $t_{off,min}$ yields approximately the same amount of absorbed energy for all cases (red line in Figure 4-12), on average 0,022 p.u.. On the right hand axis w_{Gen} represents the generated energy throughout the entire duration of the fault.

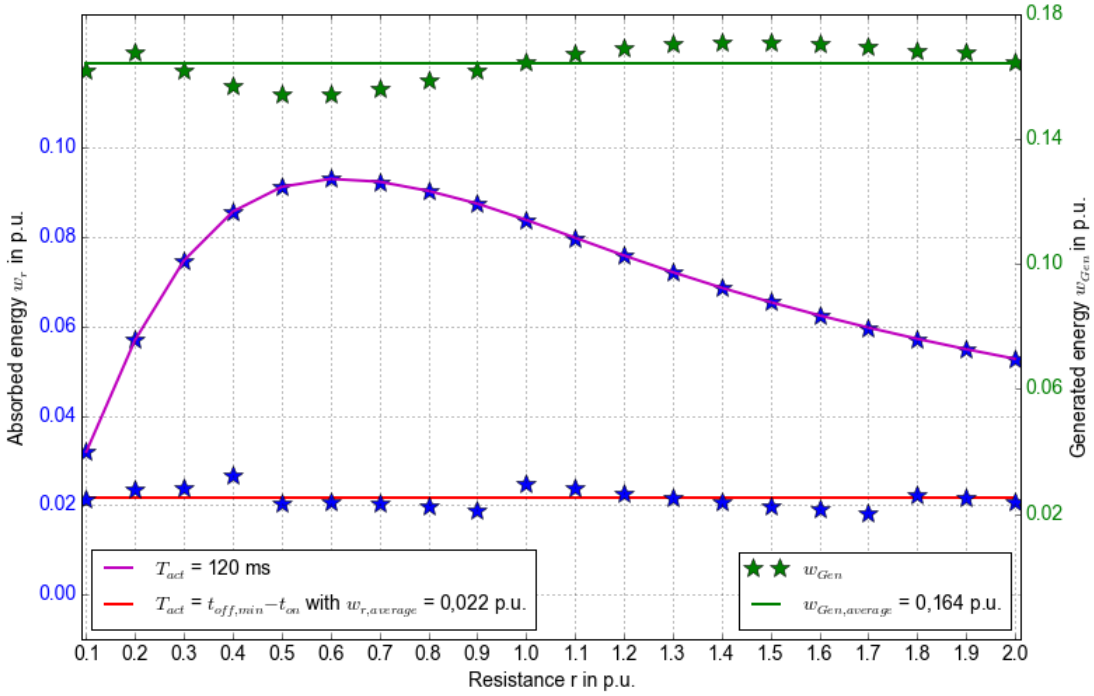

Figure 4-12: Generated vs. absorbed energy as a function of resistor value

Table 13 contains the absorbed energy in percent of the produced energy for all resistor values. A minimum ratio is achieved with a BR of 1,7 p.u. (highlighted in yellow). Hence, it can be stated that for the considered fault and pre-fault operating point at least 10,81% of the generated power have to be consumed by the resistor to avoid instability. The selected resistor absorbs 13,33%.

Table 13: Absorbed energy with respect to generated energy

r	W_r/W_{Gen}	r	W_r/W_{Gen}
p.u.	%	p.u.	%
0,1	13,13	1,1	14,23
0,2	13,99	1,2	13,46
0,3	14,79	1,3	12,77
0,4	17,12	1,4	12,17
0,5	13,33	1,5	11,65
0,6	13,37	1,6	11,19
0,7	12,99	1,7	10,81
0,8	12,39	1,8	13,31
0,9	11,71	1,9	12,84
1,0	15,10	2,0	12,57

4.4 Results

Figure 4-13 depicts the stability regions of the original setup and the modified arrangement using a BR.

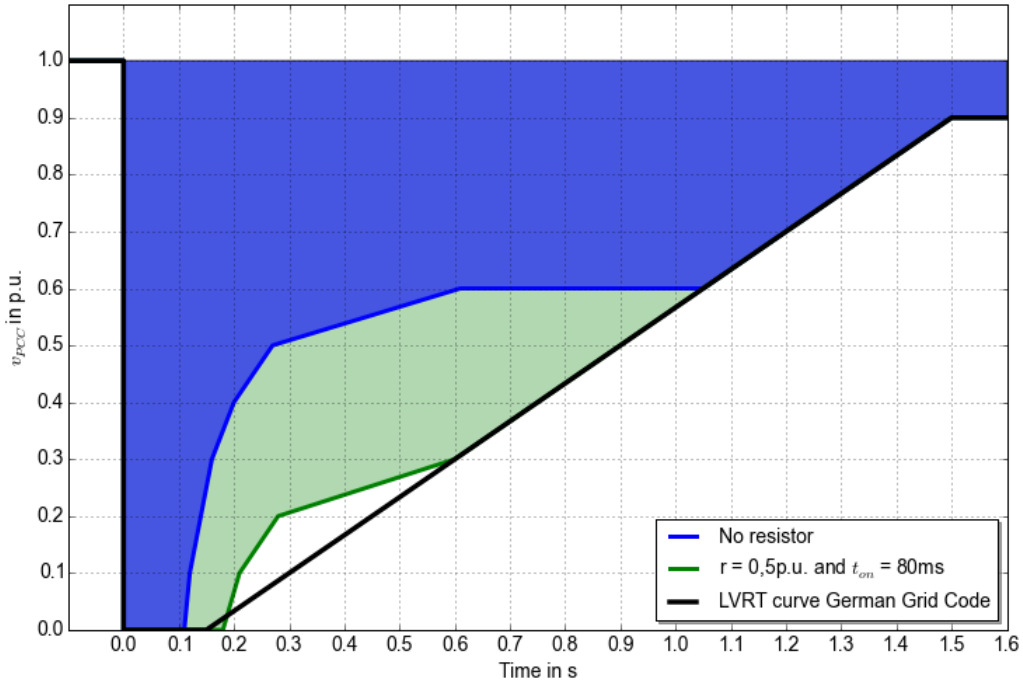

Figure 4-13: Improved stability using a BR (P = 21,7MW and pf = 0,9 under-excited)

It can be seen that the generator's FRT performance is significantly improved. Nonetheless, the definitions of the critical faults are too stringent in the German GC and cannot be fulfilled for the examined operating point.

Table 14: Stability margins for critical faults and varying power factor

P_{Gen}	$\cos(\varphi_{Gen})$	v_{PCC}	t_{cc}	M_t
MW	**under-excited**	**p.u.**	**ms**	**%**
21,7	0,9	0,1	210	-30
21,7	0,9	0,2	280	-37,8
21,7	0,95	0,1	280	-6,7
21,7	0,95	0,2	420	-6,7

Compared to the setup without improvement measures, the stability margin for the critical faults can be improved by 50% for the worst case as shown in Table 14. Even though increasing excitation entails a stabilizing effect, a power factor of 0,95 leading is still not sufficient enough to ensure GC compatibility. The machine's transient behavior is fully consistent with the German GC for all remaining operating points by adjusting the CB closing time.

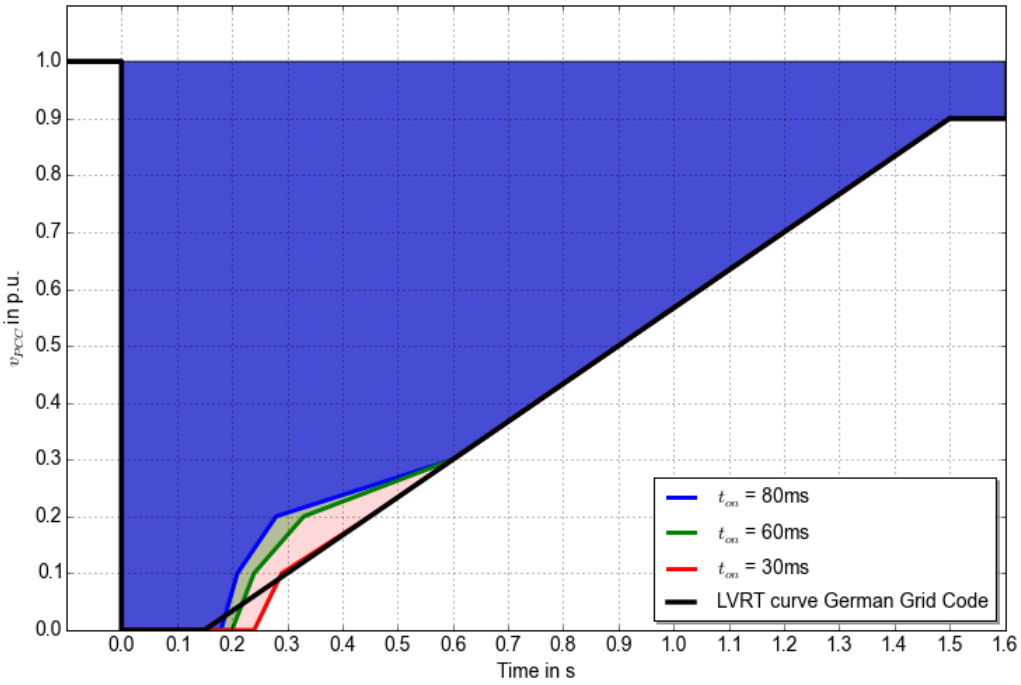

Figure 4-14: Worst case stability region as a function of resistor activation time

Decreasing the activation time t_{on} of the resistor constitutes the only measure that can significantly influence and further improve the machine's dynamic response to severe faults. Figure 4-14 demonstrates the impact of various t_{on} values on the stability region. It is evident that activation times below 30 ms are required to cover all cases. However, switching times less than 80 ms are technically not feasible for this setup.

Table 15: Minimum CB closing time $t_{off,min}$

P = 21,7 MW								
Q_{Gen}	$\cos(\varphi_{Gen})$	v_{PCC} in p.u.						
Mvar	-	0	0,1	0,2	0,3	0,4	0,5	0,6
-10,5	0,9	210 ms	x	x	490 ms	380 ms	270 ms	100 ms
-7,13	0,95	140 ms	x	x	370 ms	310 ms	200 ms	-
0	1	90 ms	230 ms	270 ms	280 ms	230 ms	-	-
7,13	0,95	-	180 ms	210 ms	260 ms	150 ms	-	-
10,5	0,9	-	160 ms	200 ms	340 ms	120 ms	-	-

The CB closing time and hence the duration throughout which the resistor remains in the circuit generally declines with increasing power factor. Care must be taken in over-excited operation where the switching time is subject to time restrictions. While in under-excited mode the resistor path may remain active (i.e. the CB open) during the simulation of 10 s without major repercussions, a loss of synchronism is detected otherwise if the resistor is not deactivated on time. Table 16 contains the maximum resistor deactivation time that can be detected.

Table 16: Maximum CB closing time $t_{off,max}$

P = 21,7 MW						
Q_{Gen}	$\cos(\varphi_{Gen})$	v_{PCC} in p.u.				
Mvar	-	0	0,1	0,2	0,3	0,4
0	1	-	-	-	590 ms	700 ms
7,13	0,95	-	-	450 ms	450 ms	220 ms
10,5	0,9	-	-	380 ms	400 ms	200 ms

The influence of different CB closing times is evident in Figure 4-15 and Figure 4-16. The results are shown for a fault with 20% remaining voltage at an over-excited power factor of 0,9. A longer insertion duration of the resistor entails a stronger braking effect. The rotor speed and angle decrease significantly, approaching the lower stability boundary (blue curve). It can also be observed that in both cases the acceleration of the rotor increases again as soon as the resistor is deactivated.

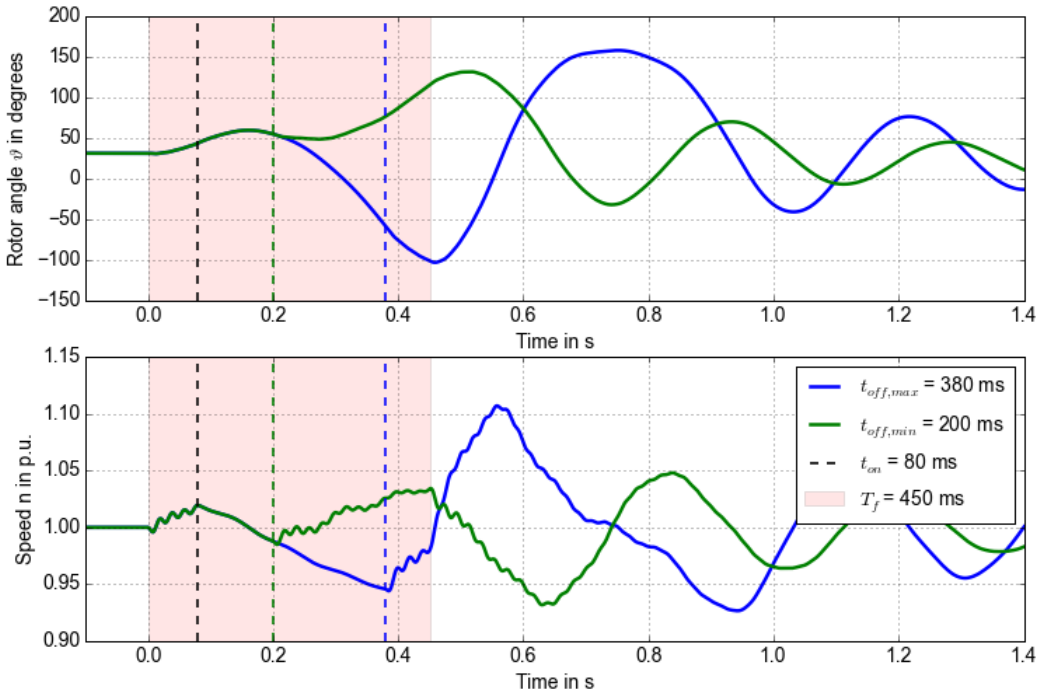

Figure 4-15: Influence of different CB closing times on rotor angle and rotor speed (v_{PCC} = 0.2 p.u.)

Figure 4-16 depicts the generated active power. Depending on the half cycle during which the fault is deactivated, the active power and thus the generator current will either instantaneously rise or fall.

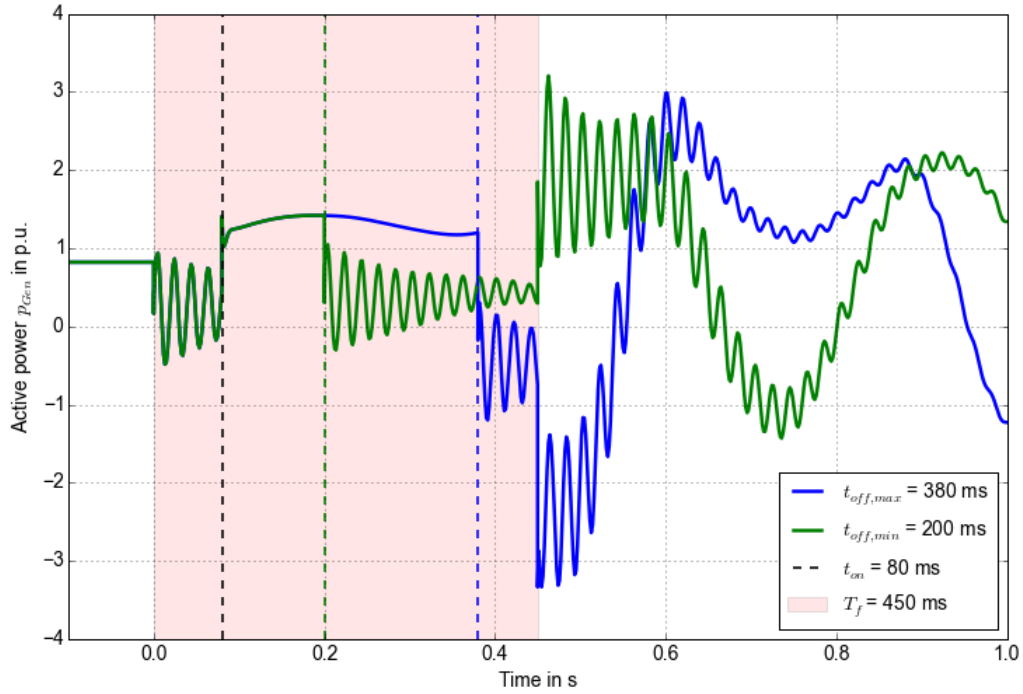

Figure 4-16: Influence of different CB closing times on generated active power (v_{PCC} = 0.2 p.u.)

The damping and stabilizing effect of a BR is shown in Figure 4-17 where a fault with 0 p.u. remaining voltage is simulated with and without stability enhancement measures.

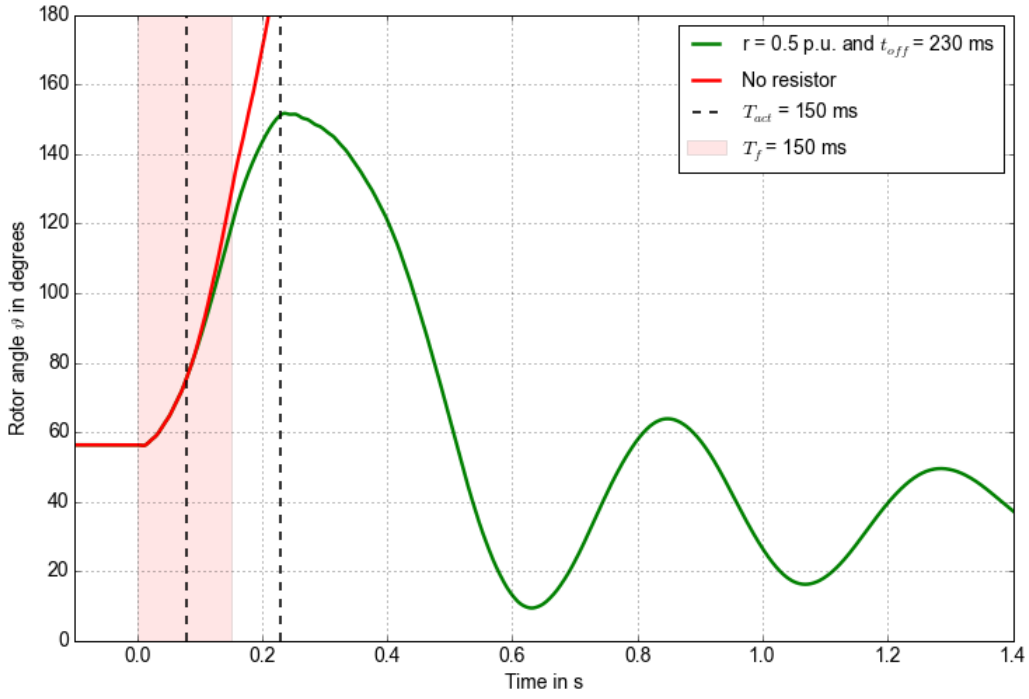

Figure 4-17: Influence of BR on rotor angle (v_{PCC} = 0.0 p.u., P = 21,7 MW an d pf = 0,9 under-excited)

Measurement devices are implemented at every bus bar. The difference between the active power signals at Gen (blue) and P1 (green) constitutes the active power losses caused by the resistor (Figure 4-18). Otherwise, when the resistor is deactivated, the two signals are equal.

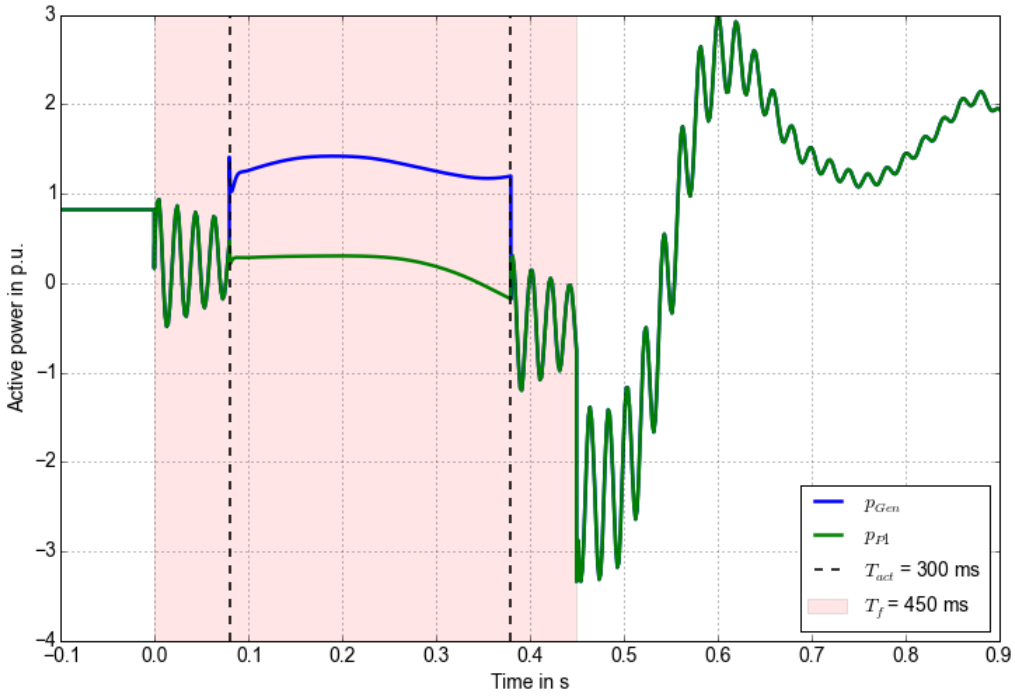

Figure 4-18: Active power measured at Gen and P1 bus bar (P = 21,7 MW and pf = 0,9 over-excited)

5 Discussion and Conclusion

5.1 Simulation environments

It has been shown that the deviations in the simulation results between OpenModelica and PowerFactory are negligibly small. Considering the uncertainties that power system studies are anyway afflicted with, it can be stated that the results are the same. Nonetheless, there are a few factors included in the OpenModelica model that obviously do beneficially influence generator stability.

The impact of the hydraulic system, the stator flux transients as well as the saturation of the stator leakage reactance have been demonstrated in this thesis. Another possible reason for differences in the post-fault recovery is the behavior of the excitation system.

It can be concluded that LVRT studies do not require detailed modelling of the system under test. RMS simulations and constant torque models provide results that are accurate enough with regard to requirements defined at the PCC level.

5.2 Series braking resistor

A series braking resistor connected to the generator output terminal has proven by transient simulations to significantly improve the LVRT performance of the bulb generator. However, certain pre-fault operating points (namely, high loading and under-excited operation) do not fulfill all the requirements of neither the German nor the Nordic GC. While critical faults occur with 10% and 20% remaining voltage in case of the E-ON GC, the Scandinavian one proves to be most demanding for faults in the range of 0% to 15%. Balanced faults leading to such severe voltage sags in all three phases are very unlikely to occur, though.

Four out of 57 cases, i.e. 7,02%, examined in this thesis that require additional stability enhancement measures for fulfilling the German GC do not achieve compliance by means of resistive braking (Table 14). This portion decreases however, when taking the probability of such severe faults into account and considering that synchronous generators are usually operated in over-excited mode.

Simulations show that a 0,5 p.u. resistor turns out to be most favorable. SBRs of 0,4 p.u. and 0,6 p.u. would reveal similar results but require longer insertion durations increasing the thermal losses. The dissipated energy determines the size and cost of the resistor and is to be optimized by adjusting the CB closing time. Another parameter to be minimized is the activation time of the resistor. As already discussed, insertion times of less than 80 ms are technically not feasible for the considered setup. However, care should be taken not to place the circuit breaker on the transformer’s high voltage side which would give rise to even higher insertion times. Often bypass switches are installed in the neutral of the generator step-up transformer to reduce insulation and switch requirements [3].

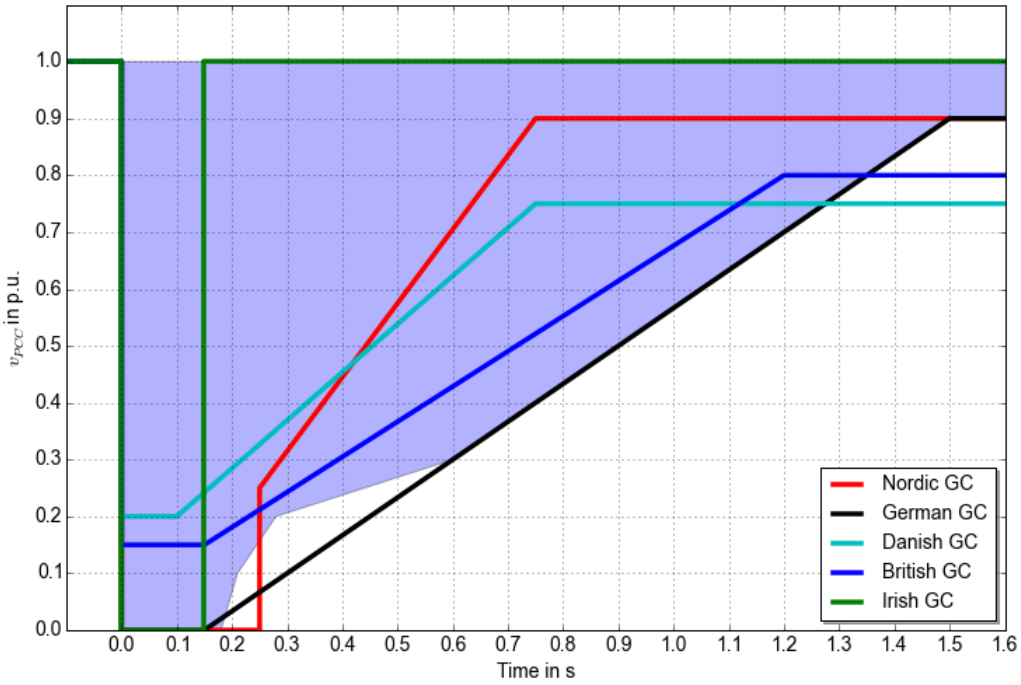

Figure 5-1: Stability region compared to various GCs (P = 21,7 MW and pf = 0,9 under-excited)

Shortcomings regarding GC compatibility are compensated for in consideration of the advantages. Uncomplicated control mechanisms, inherent self-stabilizing behavior and simple integration that do not require changes in the mechanical structure or the drive train are beneficial from both a technical as well as economic perspective. However, the best approach to effectively improve stability is a combination of several enhancement methods. High speed excitation system for example, can yield significant improvements with regard to increasing the synchronizing power during a transient disturbance. When the generator terminal voltage is low, the AVR responds by increasing the generator field voltage to the highest possible value. Excitation systems with high ceiling voltages and fast response rates supplemented with a PSS are most effective.

The stability criterion applied in this thesis solely considers rotor angle limitations. The ability to withstand voltage depressions, however, highly depends on other factors, such as the condition of protection devices including stator current and excitation current limiters.

TSOs are often criticized for trivializing the complex phenomenon of power system transient stability. The suitability of the approach to define generator fault ride through capability in simple terms by setting a voltage against time profile primarily designed for wind generators and subsequently imposed to other synchronous generators, is to be questioned. The requirements of existing GCs are often referred to rated operation of the generating unit and need to be extended and adjusted to the whole operating range. The on-going effort of the ENTSO-E to harmonize different European GCs and to address issues that have not been considered so far are crucial to future developments.

6 References

[1] ENTSO-E, *Network Code For Requirements For Grid Connection Applicable To All Generators - Frequently Asked Questions,* Brussels, 2012.

[2] DIgSILENT GmbH, *TechRef ElmSym V6,* Gomaringen, 2010.

[3] P. Kundur, Power System Stability and Control, McGraw-Hill , 1994.

[4] S. N. Vukosavic, Electrical Machines, New York: Springer , 2013.

[5] M. Ghandhari, "Stability of Power Systems," Royal Institute of Technology (KTH), Stockholm, 2013.

[6] H. Renner, "Regelung und Stabilität elektrischer Energiesysteme," Institute of Electrical Power Systems, Graz, 2010.

[7] C. Nicolet, "Hydroacoustic modelling and numerical simulation of unsteady operation of hydroelectric systems," EPFL, Lausanne, 2007.

[8] DIgSILENT GmbH, *TechRef Two-Winding Transformer (3-Phase),* Gomaringen, 2007.

[9] L. Fickert, "Grundlagen der elektrischen Energiesysteme," Institute of Electrical Power Systems, Graz, 2010.

[10] DIgSILENT GmbH, *TechRef ElmXnet,* Gomaringen, 2013.

[11] F. Iov, A. D. Hansen and P. Sorensen, "Mapping of grid faults and grid codes," Riso National Laboratory, Roskilde, 2007.

[12] N. Essl and H. Renner, "LVRT-Retardation-Device for Decentralized Power Plants," in *Electric Power Quality and Supply Reliability Conference* , Rakvere, 2014.

[13] ENTSO-E, "ENTSO-E Network Code for Requirements Applicable to all Generators," Brussels, 2013.

[14] L. Rouco, K. Chan, J. Oesterheld and S. Keller, "Recent Evolution of European Grid Code Requirements and its Impact on Turbogenerator Design," in *Power and Energy Society General Meeting*, San Diego, 2012.

[15] H. Renner and M. Sakulin, "Spannungsqualität und Versorgungszuverlässigkeit," Institute of Electrical Power Systems, Graz, 2008.

[16] M. Östman, N. Wägar, I. Ristolainen and J. Klimstra, "The impact of grid dynamics on low voltage ride through capabilities of generators," in *PowerGrid Europe 2010*, 2010.

[17] A. Causebrook, D. J. Atkinson and A. G. Jack, "Fault Ride-Through of Large Wind Farms Using Series Dyanmic Breaking Resistors," *IEEE Transactions on Power Systems ,* vol. 22, no. 3, 2007.

[18] H. Renner, M. Weixelbraun and H. Ergun, "ECOBulb Dunvegan 40 x 2.4MA Low Voltage Ride-Through study," Institute of Electrical Power Systems, Graz, 2009. Im Auftrag der Andritz Hydro GmbH.

[19] "Generator Fault Ride Through (FRT) Investigation," Transpower New Zealand Limited, 2009.

[20] S. M. Deshmukh, B. Dewani and S. P. Gawande, "A review of Power Quality Problems-Voltage Sags for Different Faults," *International Journal of Scientific Engineering and Technology ,* vol. 2, no. 5, 2013.

[21] H. Berndt, M. Hermann, H. D. Kreye, R. Reinisch, U. Scherer and J. Vanzetta, *TransmissionCode 2007 Network and System Rules of the German Transmission System Operators,* Berlin: Verband der Netzbetreiber , 2007.

[22] *Nordic Grid Code 2007 (Nordic collection of rules),* Nordel, 2007.

[23] A. Causebrook, D. J. Atkinsn and A. G. Jack, "Fault Ride-Through: Shifting the balance of power from blade pitch to electrical resistance," University of Newcastle , Newcastle .

[24] M. L. Shelton, W. A. Mittelstadt, P. F. Winkelman and W. J. Bellerby, "Bonneville Power Administration 1400-MW Braking Resistor," in *IEEE PES Summer Meeting & Energy Resources Conference* , Anaheim, 1974.

[25] P. J. Rachio, Evaluation of Dynamically Controlled Resistive Braking for the Pacific Northwest Power System, Corvallis: Oregon State University, 1994.

[26] F. M. Gonzalez-Longatt, *Tutorial: Introduction to Transient Analysis with PowerFactory,* 2009.

[27] P. Fritzson, "Modelica - A cyber-physical modeling language and the OpenModelica environment," in *7th International Wireless Communication and Mobile Computing Conference* , 2011.

[28] Z. De Greve, M. Delhaye, G. Lossa and F. Vallee, "Contribution to the Determination of the Stator Leakage Reactance of Synchronous Generators," in *International Conference on Industrial Technology* , Cape Town, 2013.

[29] M. Shan and D. Duckwitz, "Synchronous Generator System with Enhanced Capabilities for Low Voltage Ride Fault Ride Through," Fraunhofer IWES, Kassel.

7 Appendix

7.1 Appendix Chapter 3

Figure 7-1: Transformer specification plate

7.1.1 Stability regions for P = 17,8 MW and P = 13,1 MW

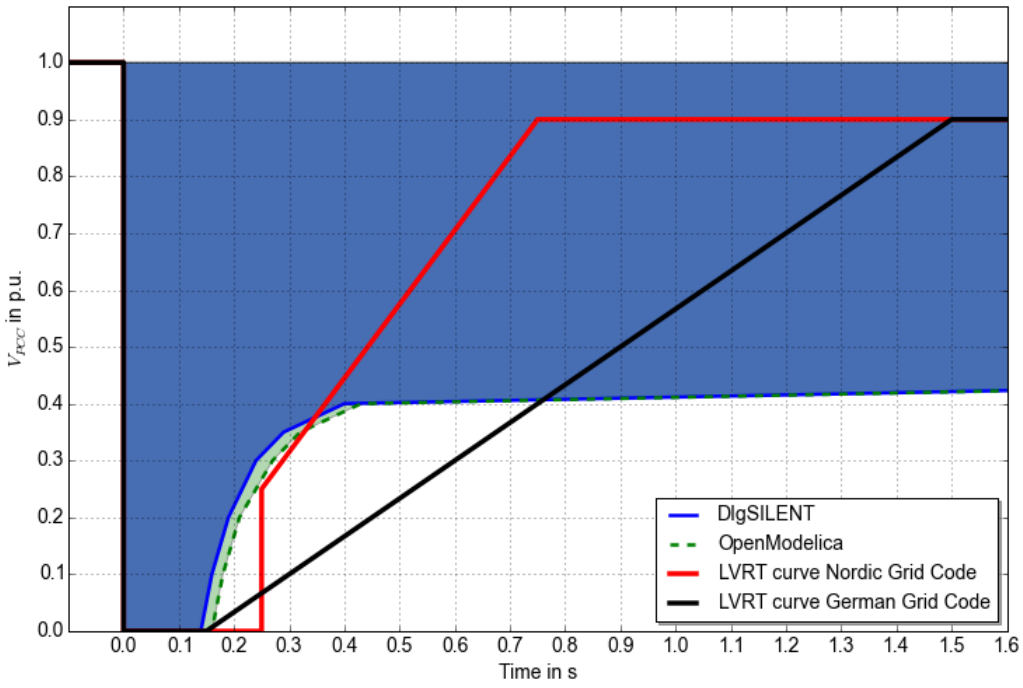

Figure 7-2: Stability region 21,7MW and pf = 0,9 over-excited

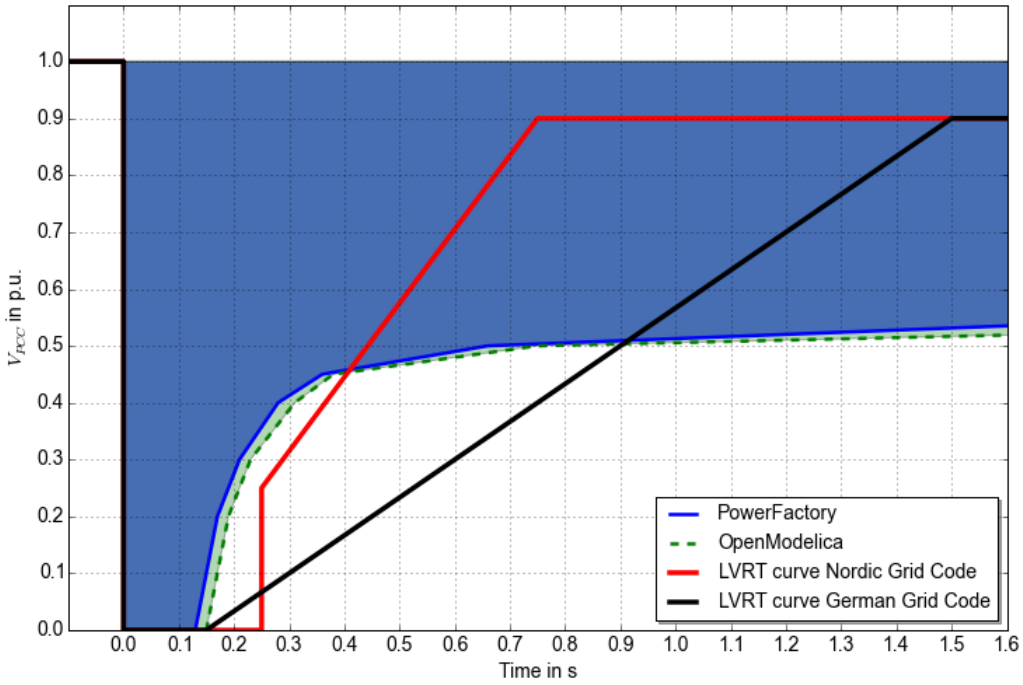

Figure 7-3: Stability region 17,8MW and pf = 0,9 under-excited

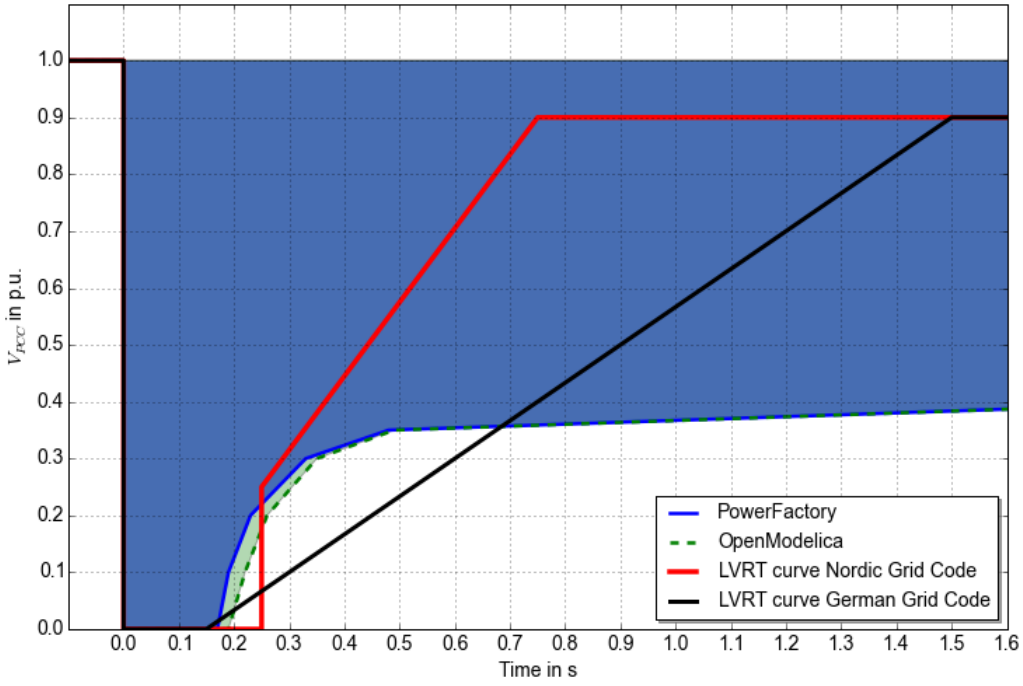

Figure 7-4: Stability region 17,8MW and pf = 0,9 over-excited

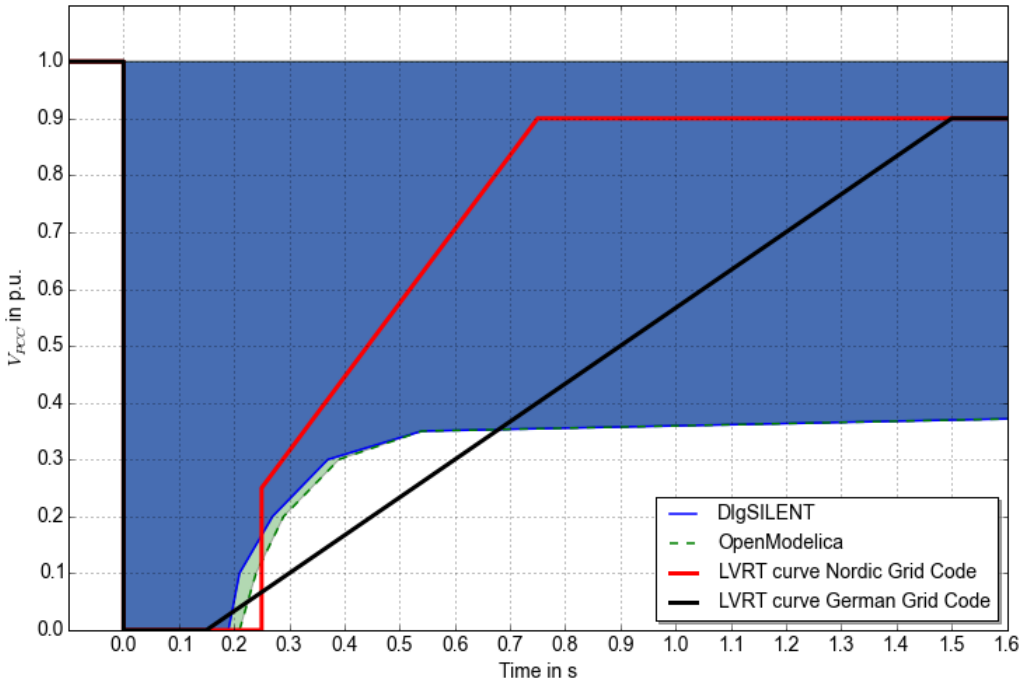

Figure 7-5: Stability region 13,1MW and pf = 0,9 under-excited

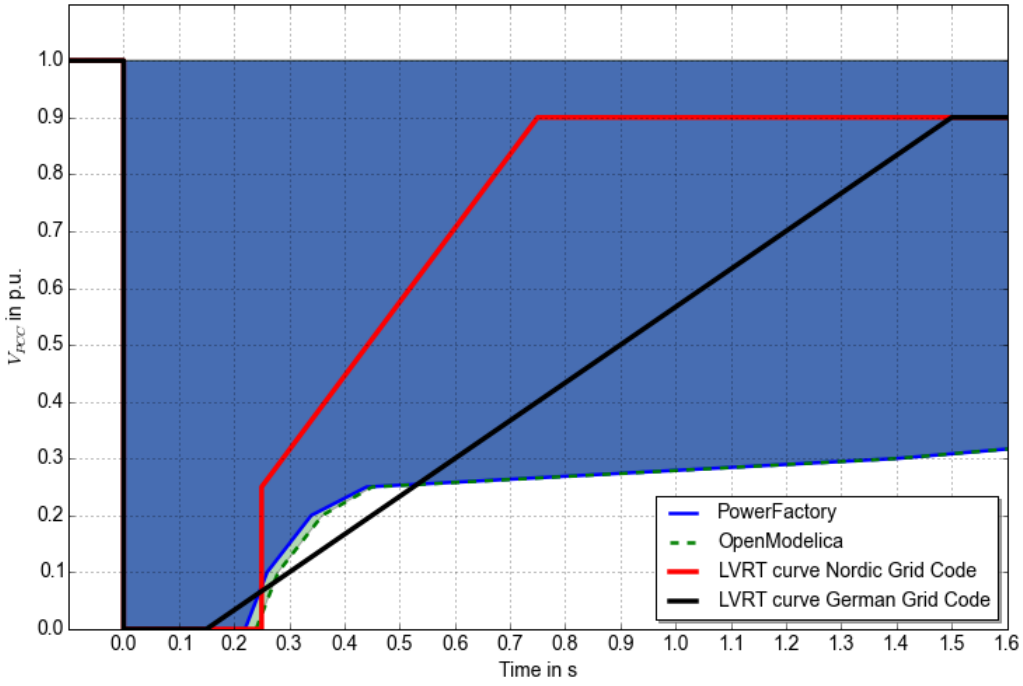

Figure 7-6: Stability region 13,1MW and pf = 0,9 over-excited

7.2 Appendix Chapter 4

7.2.1 Insertion of BR and switching times

7.2.1.1 P = 17,8 MW

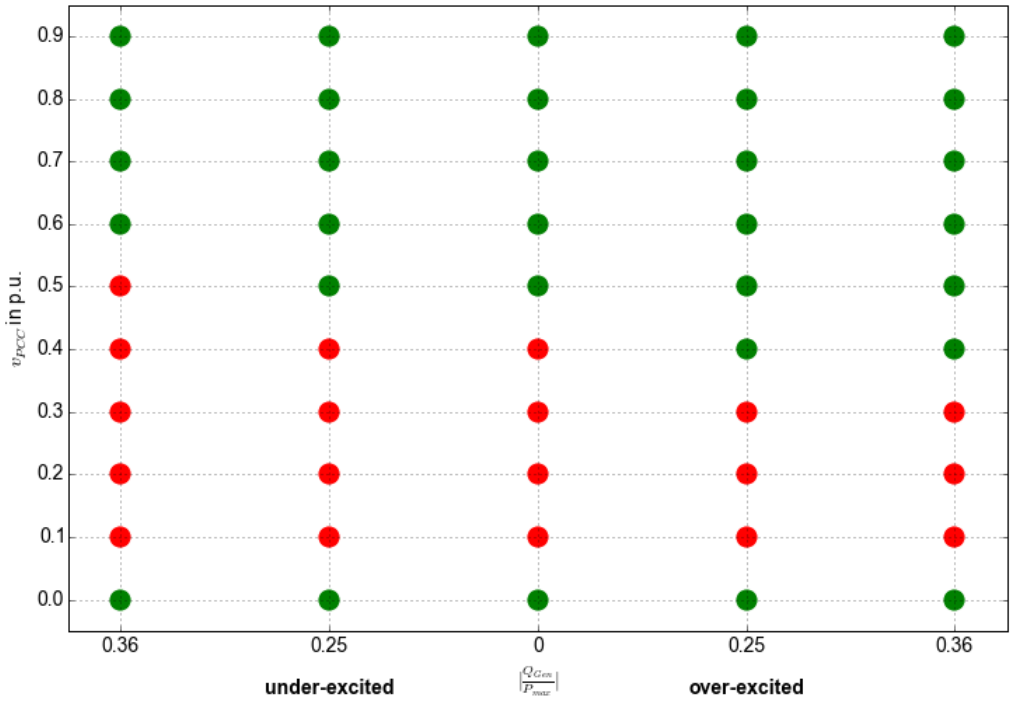

Figure 7-7: Faults requiring insertion (P = 17,8 MW)

Table 17: Minimum CB closing time $t_{off,min}$ (P = 17,8 MW)

P = 17,8 MW							
Q_{Gen}	Q_{Gen}/P_{max}	$\cos(\varphi_{Gen})$	v_{PCC} in p.u.				
Mvar	VA/W	-	0,1	0,2	0,3	0,4	0,5
-8,6	-0,36	0,9 ue	290 ms	350 ms	320 ms	250 ms	90 ms
-5,85	-0,25	0,95 ue	230 ms	290 ms	280 ms	200 ms	-
0	0	1	170 ms	220 ms	220 ms	120 ms	-
5,85	0,25	0,95 oe	140 ms	180 ms	170 ms	-	-
8,6	0,36	0,9 oe	130 ms	160 ms	150 ms	-	-

7.2.1.2 P = 13,1 MW

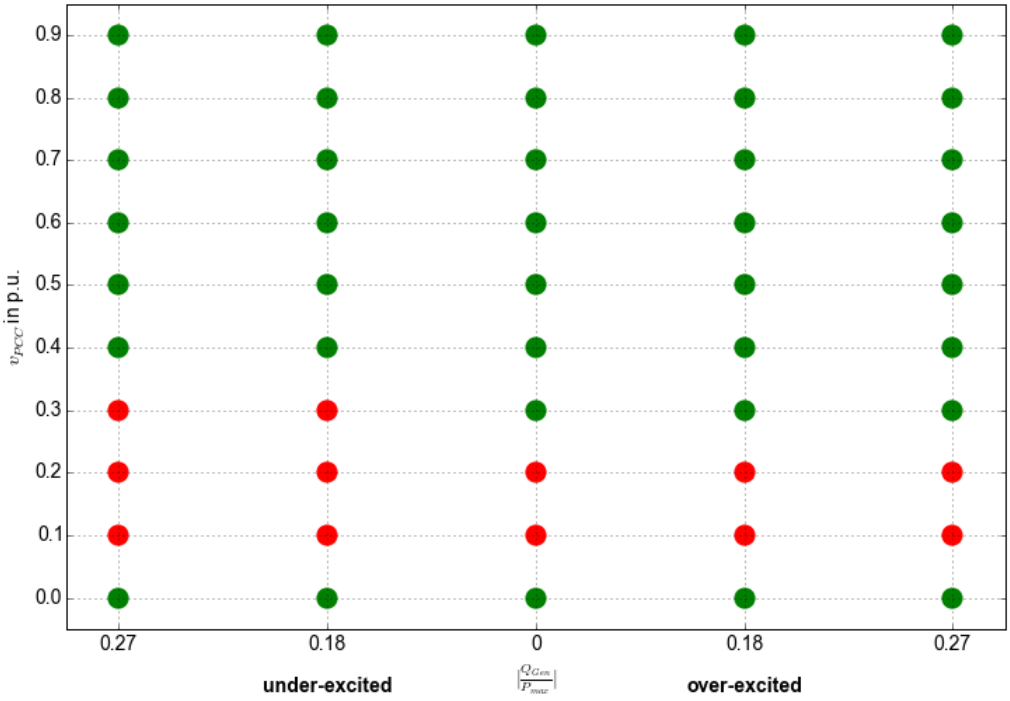

Figure 7-8: Faults requiring insertion (P = 13,1 MW)

Table 18: Minimum CB closing time $t_{off,min}$ (P = 13,1 MW)

P = 13,1 MW					
Q_{Gen}	Q_{Gen}/P_{max}	$\cos(\varphi_{Gen})$	v_{PCC} in p.u.		
Mvar	VA/W	-	0,1	0,2	0,3
-6,35	**-0,27**	**0,9 ue**	140 ms	190 ms	170 ms
-4,31	**-0,18**	**0,95 ue**	130 ms	170 ms	150 ms
0	**0**	**1**	110 ms	140 ms	-
4,31	**0,18**	**0,95 oe**	100 ms	120 ms	-
6,35	**0,27**	**0,9 oe**	90 ms	110 ms	-